CrossMark

ORIGINAL PAPER

Postcollisional cooling history of the Eastern and Southern Alps and its linkage to Adria indentation

Bianca Heberer[1] · Rebecca Lee Reverman[2,3] · Maria Giuditta Fellin[4] ·
Franz Neubauer[1] · István Dunkl[5] · Massimiliano Zattin[6] · Diane Seward[7] ·
Johann Genser[1] · Peter Brack[2]

Abstract Indentation of rigid blocks into rheologically weak orogens is generally associated with spatiotemporally variable vertical and lateral block extrusion. The European Eastern and Southern Alps are a prime example of microplate indentation, where most of the deformation was accommodated north of the crustal indenter within the Tauern Window. However, outside of this window only the broad late-stage exhumation pattern of the indented units as well as of the indenter itself is known. In this study we refine the exhumational pattern with new (U–Th–Sm)/He and fission-track thermochronology data on apatite from the Karawanken Mountains adjacent to the eastern Periadriatic fault and from the central-eastern Southern Alps.

Apatite (U–Th–Sm)/He ages from the Karawanken Mountains range between 12 and 5 Ma and indicate an episode of fault-related exhumation leading to the formation of a positive flower structure and an associated peripheral foreland basin. In the Southern Alps, apatite (U–Th–Sm)/He and fission-track data combined with previous data also indicate a pulse of mainly Late Miocene exhumation, which was maximized along thrust systems, with highly differential amounts of displacement along individual structures. Our data contribute to mounting evidence for widespread Late Miocene tectonic activity, which followed a phase of major exhumation during strain localization in the Tauern Window. We attribute this exhumational phase and more distributed deformation during Adriatic indentation to a major change in boundary conditions operating on the orogen, likely due to a shift from a decoupled to a coupled system, possibly enhanced by a shift in convergence direction.

✉ Bianca Heberer
  bianca.heberer@sbg.ac.at

1 Department of Geography and Geology, University of Salzburg, Hellbrunner Str. 34, 5020 Salzburg, Austria

2 Geological Institute, ETH Zürich, Sonneggstrasse 5, 8092 Zurich, Switzerland

3 Department of Earth and Planetary Sciences, University of California, Berkeley, Berkeley, CA 94720, USA

4 Institute for Geochemistry and Petrology, ETH Zürich, Clausiusstrasse 25, 8092 Zurich, Switzerland

5 Geoscience Center, University of Göttingen, Goldschmidtstrasse 3, 37077 Göttingen, Germany

6 Department of Geosciences, University of Padua, Via G. Gradenigo 6, 35131 Padua, Italy

7 School of Geography, Environment and Earth Sciences, Victoria University of Wellington, PO Box 600, Wellington 6012, New Zealand

Introduction

Late-orogenic indentation by rigid lithospheric plates and microplates into a weaker continent leads to postcollisional shortening, lithospheric thickening, vertical and lateral extrusion and erosion (e.g., Robl and Stüwe 2005; Tapponnier et al. 1986). The European Eastern Alps are a prime example of microplate indentation (Ratschbacher et al. 1991). Their Late Neogene geodynamic framework is influenced primarily by the ca. NW-ward motion of the Adriatic plate and its counterclockwise rotation with respect to Europe, which resulted in an oblique, dextral transpressional setting (e.g., Caputo and Poli 2010; Scharf
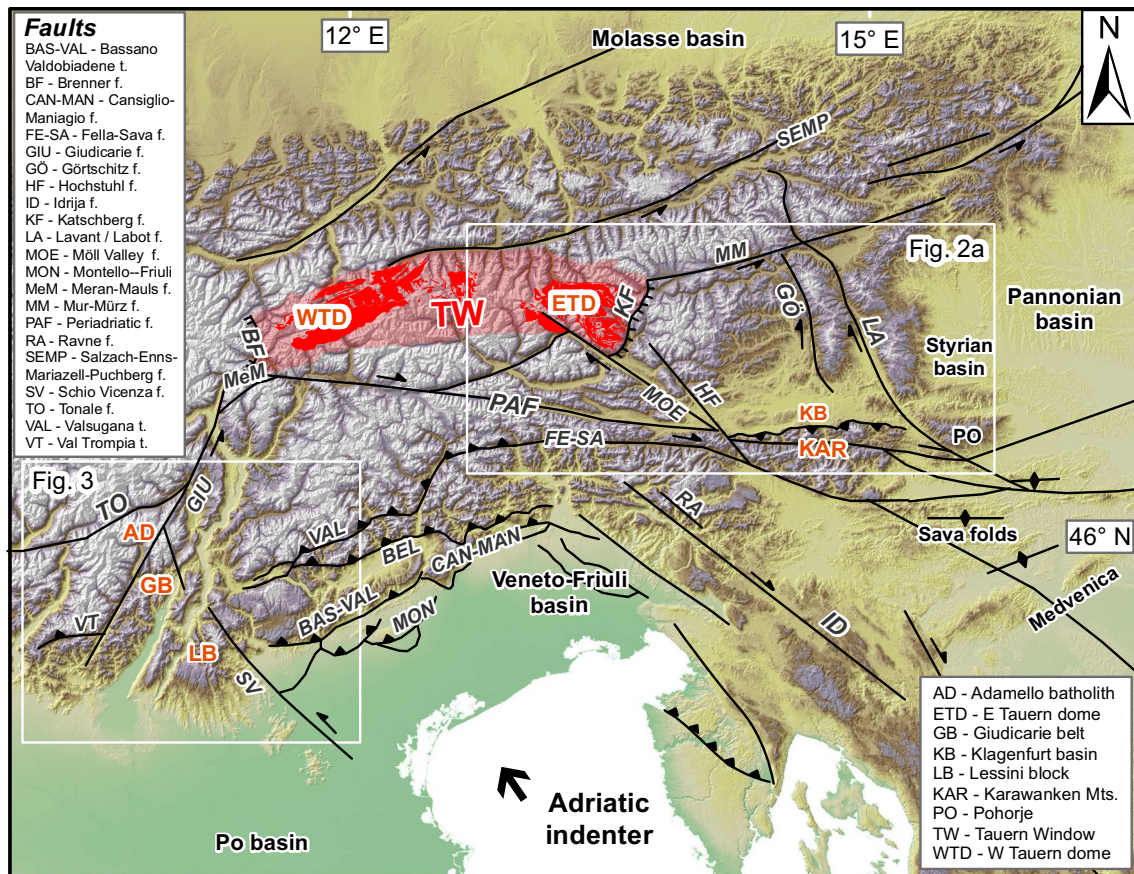
Fig. 1 DEM of the Southern Alps, Eastern Alps and northern Dinarides displaying major faults. The *dark red* signature within the Tauern Window denotes outcropping "Zentralgneiss" of the Tauern subdomes. *Frames* denote outline of Figs. 2a and 3

et al. 2013). The northern edge of the Adriatic indenter roughly corresponds to the Periadriatic fault system (PAF, Fig. 1), the largest, most important discontinuity and the main structural divide of the European Alps. The PAF system is offset by the sinistral NE–SW trending transpressive Giudicarie fault, which defines the western border of the eastern Adriatic indenter (sensu Handy et al. 2014), i.e., the still northward moving triangular northeastern part of the Southalpine block that indented the Eastern Alps (also labeled North Adriatic indenter by, e.g., Massironi et al. (2006), Southalpine indenter by, e.g., Pomella and Stipp (2012), or Dolomites indenter by Frisch et al. (2000), among others). The onset of indentation occurred at ca. 23–21 Ma (Pomella and Stipp 2012; Scharf et al. 2013).

The bulk of Adriatic plate motion was transferred into differential deformation north and south of the PAF system. Exhumation and deformation north of the PAF primarily occured in the axial zone of the orogen in the Tauern Window, where between 23 and 21 Ma deep, high-pressure units (the Penninic nappes) started to exhume to shallow

crustal depths via orogen-parallel extension (e.g., Behrmann 1988; Scharf et al. 2013) (Figs. 1, 2). Exhumation continued until the Late Miocene leading to the formation of large-amplitude folds and domes in the Tauern Window (e.g., Schmid et al. 2013). South of the PAF system, limited exhumation from shallow crustal levels (Zanchetta et al. 2015; Zattin et al. 2006) occurred, and throughout the Oligo-Miocene most deformation was accommodated by progressive southward thrust propagation and transpressional shear along the indenter margin (Picotti et al. 1995; Pomella and Stipp 2012; Prosser 1998; Viola et al. 2001). West of the Giudicarie fault, thermochronological data from the Adamello complex, the largest Tertiary intrusion of the Alps, record rapid uplift and exhumation from a shallow depth (~2 km) between 8 and 6 Ma (Reverman et al. 2012) (Fig. 3). Much less is known about the exhumation pattern at the eastern and northeastern immediate front/rim of the eastern Adriatic indenter. For the indented units north of the PAF, in particular SE and E of the Tauern Window, age data are sparse and only the broad exhumation pattern
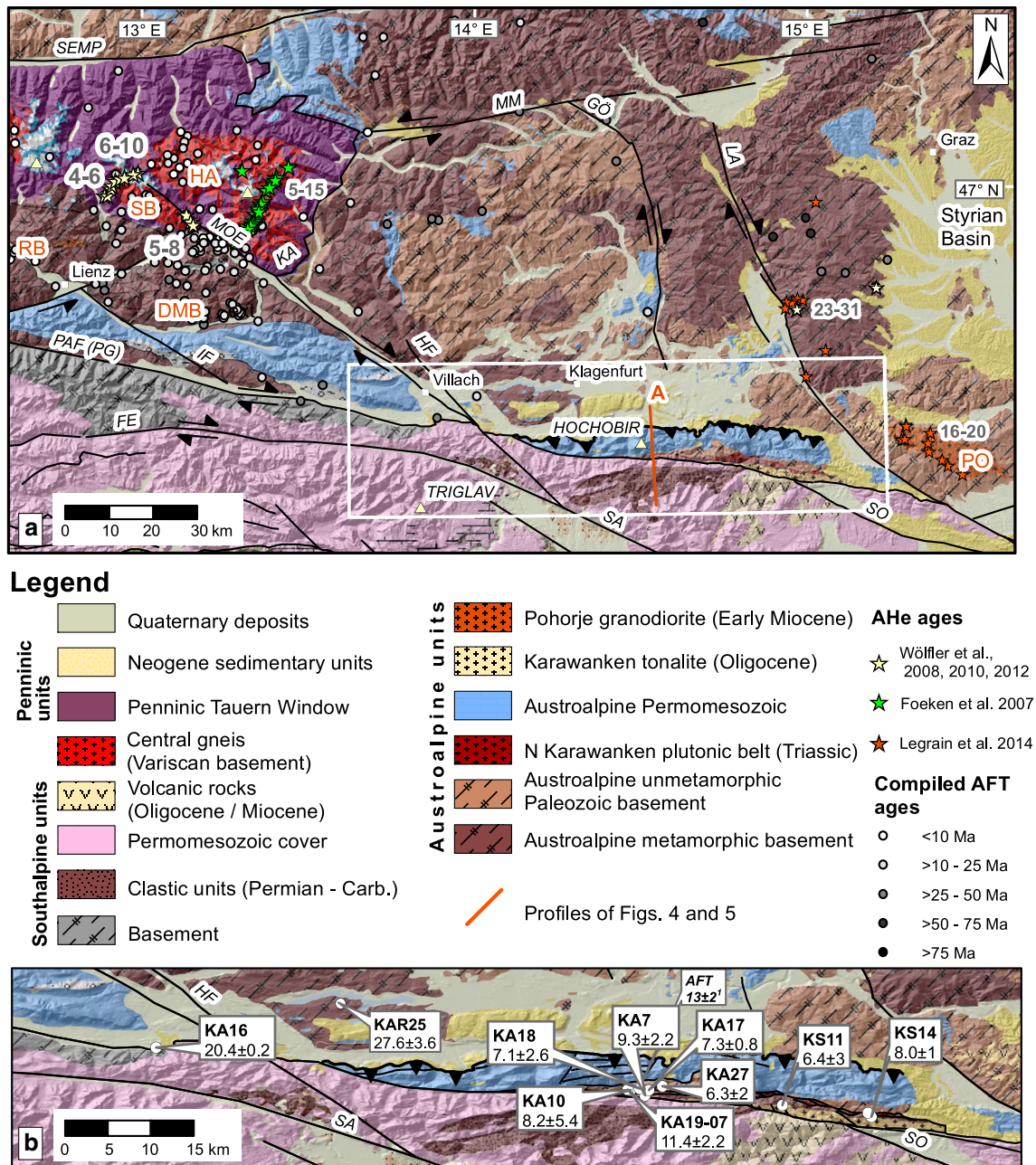
Fig. 2 a Geological map of the Eastern and Southern Alps bordering the easternmost PAF and the Karawanken Mts. illustrating major faults and summarized low-temperature thermochronology data. AFT ages were compiled from Bertrand (2013), Hejl (1997), Staufenberg (1987), Wölfler et al. (2008, 2010, 2012). *DMB* Drau-Möll block, *FE* Fella fault, *GÖ* Görtschitz fault, *HA* Hochalm–Ankogel subdome, *HF* Hochstuhl fault, *IF* Isel fault, *KA* Katschberg fault, *LA* Lavant/Labot fault, *MM* Mur-Mürz fault, *MOE* Möll Valley fault, *PAF* Periadriatic fault, *PG* Pusteria–Gailtal fault segment of the PAF, *PO* Pohorje, *RB* Rieserferner block, *SA* Sava fault, *SB* Sonnblick subdome, *SEMP* Salzach–Enns–Mariazell–Puchberg fault, *SO* Sostanj fault. *Frame* denotes outline of (**b**). **b** New AHe ages with 2σ error for the Karawanken Mountains. Referenced AFT age from [1]Nemes (1996)

is known (Hejl 1997; Staufenberg 1987; Wölfler et al. 2012) (Fig. 2a), although the Eastern Alps are tectonically more active than the Western and Central Alps due to ongoing indentation (e.g., Battaglia et al. 2004). Except for a single apatite fission-track (AFT) age from the Karawanken tonalite (Nemes 1996) (Fig. 2b), no low-temperature

thermochronological data exist for the eastern segment of the PAF system, the first focus of this study. The published age record is more abundant for the western part of the leading edge of the eastern Adriatic indenter, but mostly limited to FT data. Along the NW corner of the indenter fission-track data on apatites and zircons (ZFT) portray
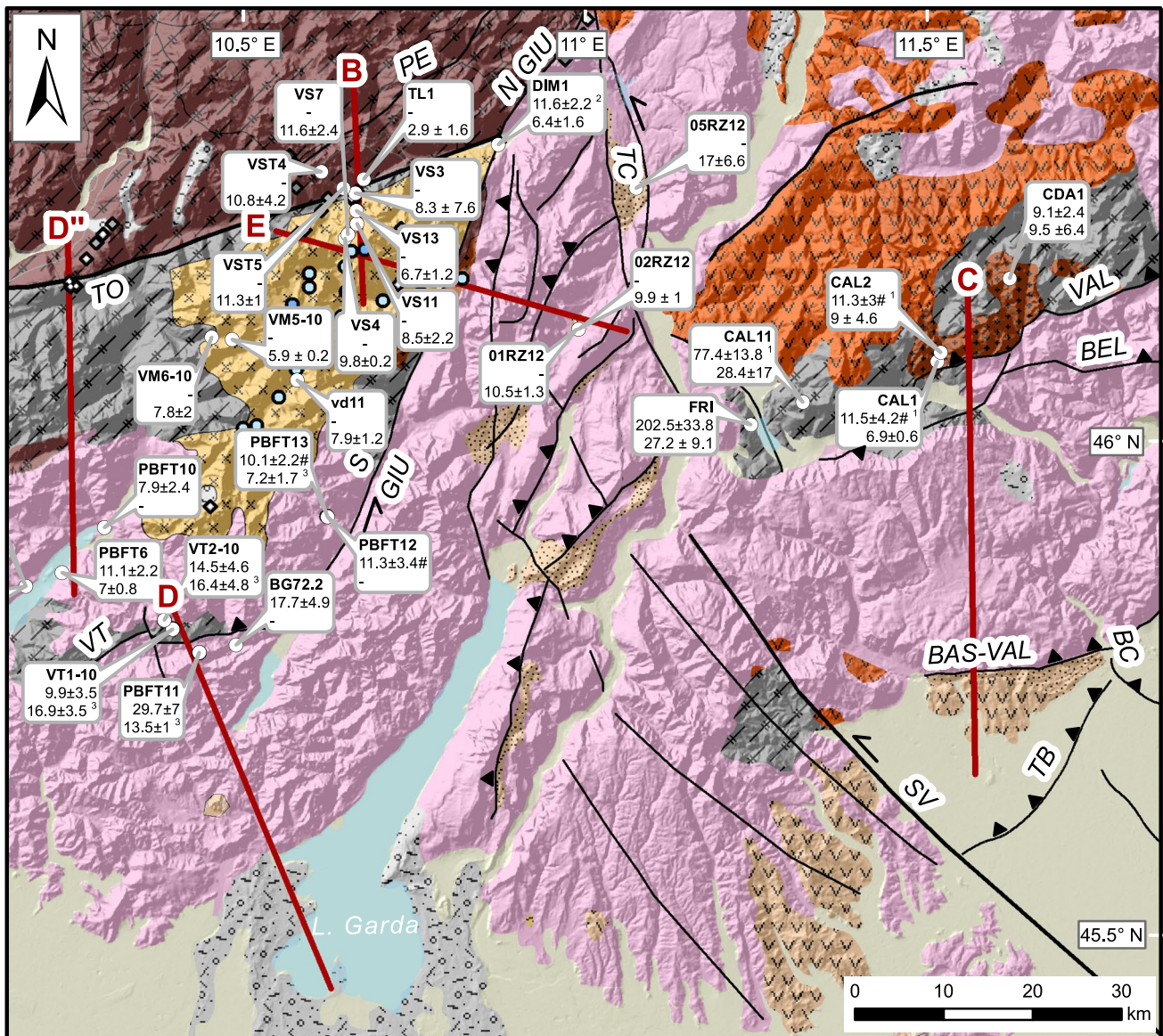
Legend

	Quaternary deposits, undiff.
	Pleistocene glacial deposits
	Austroalpine units

O — Sample locations with ages

Sample #
AFT age ± 2σ
AHe age ± 2σ

— Profiles of figs. 4 & 5

Southalpine units

	Paleogene Adamello complex
	Paleogene sedimentary units
	Tertiary volcanic rocks
	Permomesozoic cover
	Permian granitoids
	Permian volcanics
	Basement

Compiled ages
ZFT ages

◇ > 10 - 25 Ma
◈ > 25 - 40 Ma
◆ > 40 - 60 Ma
◆ > 60 Ma

AHe ages

◉ > 5 - 10 Ma
◉ > 10 - 15 Ma

◄**Fig. 3** Geological map of the Southalpine units targeted for low-temperature thermochronology. New and published AFT and AHe ages with errors given as 2σ are shown. Labeled published ages are from [1]Zattin et al. (2003, 2006); [2]Pomella et al. (2011) and [3]Reverman et al. (2012). #-Sample failed Chi-square test indicating significant dispersion in ages. ZFT ages were compiled from Pomella et al. (2011, 2012), Stipp et al. (2004), Viola (2000), Viola et al. (2001, 2003). Compiled AHe data (unlabeled) come from Reverman et al. (2012). Geology is based on the geological map of Italy, scale 1:1,250,000 (2005) and the structural model of Italy, scale 1:500.000 (Bigi et al. 1990). *BAS-VAL* Bassano–Valdobiadene thrust, *BC* Bassano–Cornuda thrust, *BEL* Belluno line, *N GIU* North Giudicarie line, *PE* Pejo fault, *S GIU* South Giudicarie line, *SV* Schio–Vicenza fault, *TB* Thiene–Bassano thrust, *TC* Trento–Cles fault, *TO* Tonale fault, *VAL* Valsugana thrust, *VT* Val Trompia thrust

a complex cooling pattern with a corridor of young Miocene ZFT ages (Pomella and Stipp 2012; Viola et al. 2001). Thermochronological data from within the indenter are again scarce due to limited availability of suitable lithologies. AFT dating of Southalpine crystalline basement in the hanging wall of a major thrust (Valsugana thrust, Fig. 3) yielded evidence for prominent Late Miocene cooling and exhumation (Zattin et al. 2006), but no constraints exist for other major structural units and new low-temperature thermochronological data are needed to bridge this gap. Thus, our second focus is on the Southern Alps, from where we present new AFT and apatite (U–Th–Sm)/He (AHe) ages that complement and enhance previous work. In particular, we focus on the Giudicarie belt and surrounding regions corresponding to the western boundary zone of the eastern Adriatic indenter.

Our goal is to capture the spatial and temporal variability of the vertical component of extrusion associated with microplate indentation and ongoing convergence during the late stages of Alpine orogeny. A better understanding of the magnitude and timing of uplift will also shed light on the discussion on the topographic evolution of the Alps (e.g., Hergarten et al. 2010; Robl et al. 2015) and its potential coupling to climate and deep-seated tectonic processes beneath the Alps (e.g., Baran et al. 2014; Cederbom et al. 2004; Fox et al. 2015; Herman et al. 2013). By recombining our new age information with the published record from the Eastern and Southern Alps and the clastic record from the peripheral foreland basin of the Karawanken Mountains we find a young, latest Mid-Miocene but predominantly Late Miocene exhumation pulse as a first-order feature of the cooling pattern. This adds a second phase of exhumation and shortening to the postcollisional evolution of the Eastern Alps, following an initial, well-known stage of Early to Middle Miocene stationary, large-amplitude exhumation concentrated in the Tauern Window (e.g., Luth and Willingshofer 2008). The spatial evolution of exhumation through time is discussed in light of Adriatic indentation.

Geological background and tectonic setting of the study areas

After the Cretaceous-to-early-Paleogene subduction and closure of the Piemontais-Ligurian ("Penninic") ocean, the Eocene-to-Oligocene collision of the stable European continent and the Adriatic microplate resulted in the building of the European Alps (e.g., Handy et al. 2010). The Adriatic indenter, i.e., the northern promontory of the Adriatic microplate (Southern Alps) had only experienced lower-greenschist-facies Alpine overprint (e.g., Spalla and Gosso 1999) and acted as a strong indenter (Robl and Stüwe 2005; Willingshofer and Cloetingh 2003). Intra-orogenic N–S shortening was largely compensated by orogenic thickening due to nappe stacking, e.g., by thrusting along a crustal-scale shear zone known as sub-Tauern ramp (Gebrande et al. 2002; Lammerer et al. 2008), followed by large-scale doming and exhumation (e.g., Favaro et al. 2015). In the Eastern Alps maximum amounts of collisional shortening occurred in the western part of the Tauern Window (Rosenberg et al. 2015). ZFT ages mostly range between 18 and 12 Ma in the Tauern Window (Bertrand et al. 2015 and references therein) and are older only in its SE corner (Dunkl et al. 2003; Staufenberg 1987). There, AFT and AHe ages are between 23 and 7 and 15 and 5 Ma, respectively (Foeken et al. 2007; Wölfler et al. 2012) (Fig. 2a).

The more than 700-km-long PAF is the most outstanding fault system of the Alps. It juxtaposes the N-vergent part of the orogen to the Southalpine retrowedge and separates terrains with distinct paleogeographic, magmatic and metamorphic development (e.g., Laubscher 1983; Schmid et al. 1987), which were, however, closely coupled since the Miocene (e.g., Massironi et al. 2006). The PAF delimits the SSE-vergent fold and thrust belt of the eastern Southern Alps to the north. The Giudicarie belt and the relatively undeformed Lessini foreland block represent the western, the NW–SE trending dextral Idria and Ravne faults (Fig. 1) its eastern boundary. The Southalpine fold and thrust belt east of the Adamello complex mainly developed during polyphase Neogene contraction and inversion of the Adriatic passive margin (Zampieri and Massironi 2007). The most important tectonic features of the eastern Southern Alps are from N to S the Valsugana, Belluno, Bassano and Montello thrust sheets, involving both basement and Permo-to-Cenozoic cover rocks. Frontal thrusts are linked via the NW–SE trending Schio-Vicenza and N–S trending Trento-Cles strike-slip faults to the Giudicarie belt (Massironi et al. 2006) (Figs. 1, 3).

The PAF system comprises various segments, i.e., from W to E the Canavese, Tonale, Giudicarie and Pusteria–Gailtal faults and its extension into the Karawanken Mountains (Fig. 1). This study targets two key areas in the vicinity of
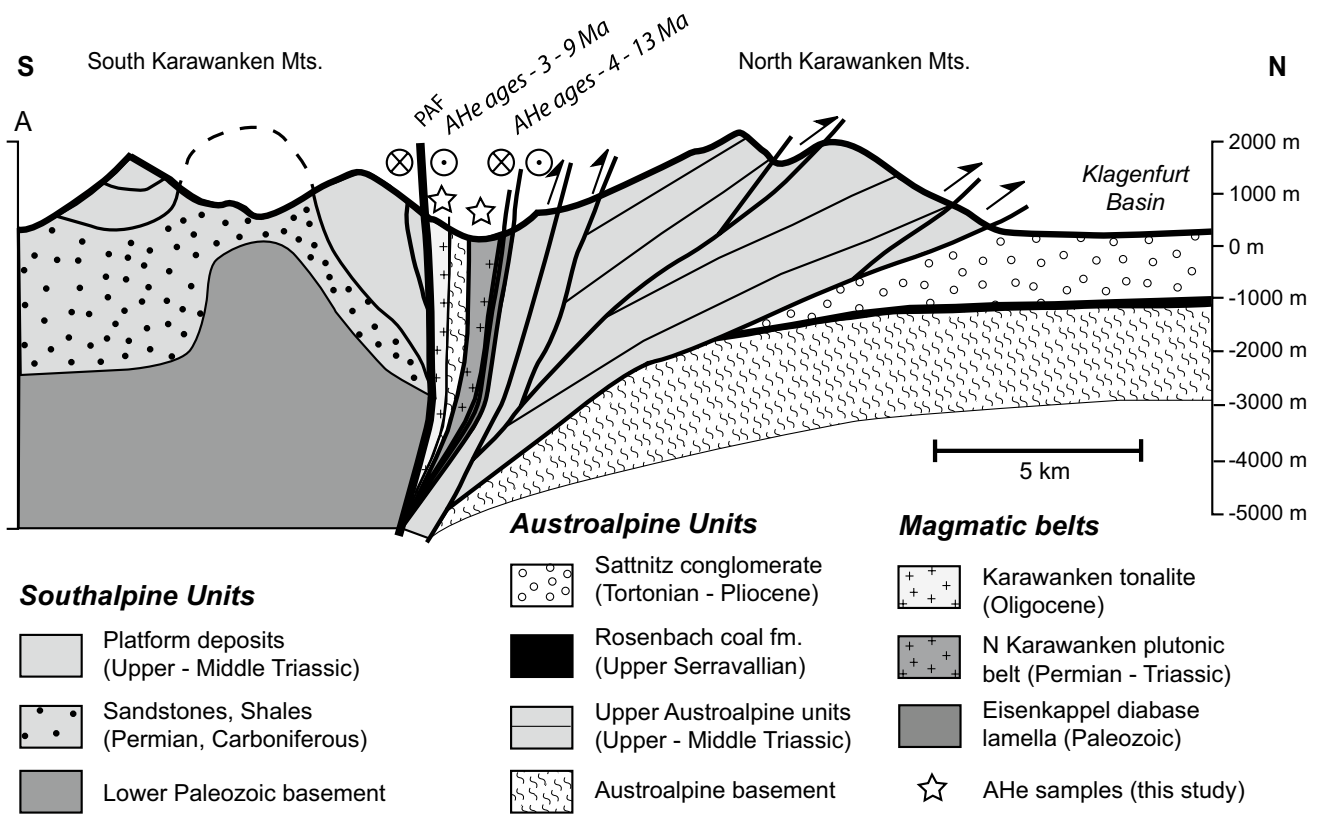
Fig. 4 S–N section across the Karawanken flower structure (modified after Nemes et al. 1997). Trace of the section is indicated in Fig. 2

the PAF system at the leading northern and western edge of the eastern Adriatic indenter (Fig. 1): (1) the easternmost PAF segment within the Karawanken Mountains and (2) the central-eastern Southern Alps. In the following, we give a brief overview for those major units targeted for low-temperature thermochronological dating.

Eastern Periadriatic fault/Karawanken Mountains

The eastern PAF system is trisected (Fig. 2): (1) A straight western segment coincides with the easternmost Pusteria–Gailtal fault. (2) The central segment is limited by the Hochstuhl–Möll Valley fault system and Lavant (Labot) fault which both offset the PAF system (ca. 4–6 km displacement, respectively, ca. 10–15 km). A positive flower structure straddles the PAF, which separates the distinct North and South Karawanken units (Laubscher 1983; Polinski and Eisbacher 1992; Tollmann 1985) (Fig. 4). (3) In the eastern segment, east of the Lavant fault, the PAF juxtaposes the Pohorje basement in the north and the Sava fold area in the south. The Sava folds were deformed by N–S shortening during Middle and Late Miocene times, leading to cooling below 110 °C from 10 to 15 Ma (Sachsenhofer et al. 2001). East of the Lavant fault, the PAF

system is buried beneath the Tertiary sediments of the Pannonian basin (Fodor et al. 1998).

The brittle dextral Hochstuhl–Möll Valley fault system links the eastern PAF with the Tauern Window (Figs. 1, 2). Structural and metamorphic basement domes of Variscan granitoids ("Zentralgneis" of the Sonnblick and Hochalm subdomes, Figs. 1, 2) within the eastern Tauern window are transected by the Möll Valley fault, which also transects the eastern PAF system (Figs. 1, 2) (Kurz and Neubauer 1996; Polinski and Eisbacher 1992; Scharf et al. 2013). During the Early-to-Middle Miocene extrusion the Möll Valley fault accommodated up to 25 km of displacement (Kurz and Neubauer 1996; Scharf et al. 2013; Wölfler et al. 2008).

In the central segment, the North Karawanken unit was overthrust onto the flexural Klagenfurt basin (Figs. 2, 4). This intra-orogenic basin comprises a more than 1000-m clastic sequence ranging from fine-grained, coal-bearing early Sarmatian (Serravalian) deposits (Klaus 1956; Tollmann 1985) to coarse-grained Pontian (Late Messinian) deposits and Pliocene to possible Pleistocene conglomerates (for details see Nemes et al. 1997 and references therein). Several large and small calc-alkaline intrusions and mafic dike swarms of Oligocene age, that were emplaced due to the break-off of the European slab (von
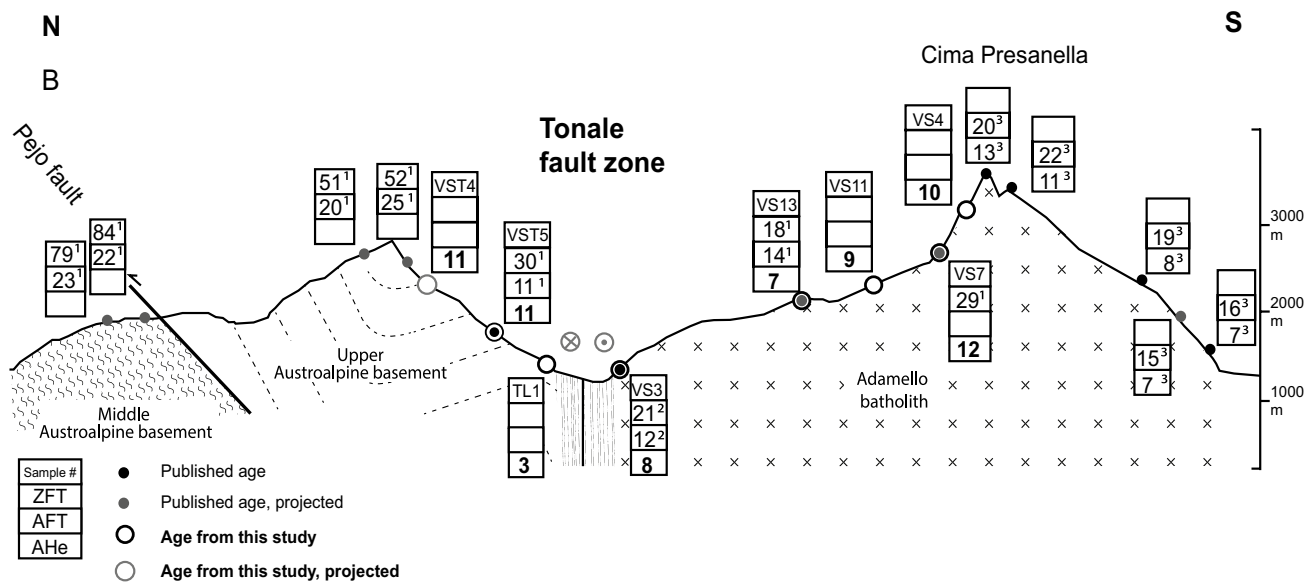
Fig. 5 N–S cross section of the Tonale fault. Published ages are from [1]Viola et al. (2003); [2]Stipp et al. (2004); [3]Reverman et al. (2012). Cross section modified after Dal Piaz et al. (2007). Trace of the section (*B*) is indicated in Fig. 3

Blanckenburg and Davies 1995), are aligned along the PAF system. The segment of the Karawanken Mountains targeted for sampling displays narrow ca. E-W trending bands of Permotriassic Eisenkappel granite (North Karawanken plutonic belt), Paleozoic metasedimentary rocks and ductilely deformed Oligocene Karawanken tonalite in the immediate vicinity of the PAF system (Fig. 4) (Cliff et al. 1974; Exner 1976; Miller et al. 2011; Scharbert 1975; von Gosen 1989).

Based on paleomagnetic data, mapping, stratigraphy and sedimentological studies, Fodor et al. (1998) provided a detailed structural framework and kinematic sequence for the Miocene–Pliocene evolution of the Slovenian part of the Periadriatic fault, just east of our study area. They differentiated an Early Miocene compression, a Karpatian transtension and a Middle Miocene-to-Quaternary compressional event. They also found a complex pattern of block rotations in the vicinity of the PAF.

Tonale fault

The Tonale fault is the central-eastern segment of the PAF system (Figs. 3, 5). Its Cenozoic kinematic history is complex and records competing effects of terminal oblique convergence and rotation of the Adriatic indenter and simultaneous orogen-parallel extension (Mancktelow 1992). The western sector of the Tonale fault, adjacent to the Bergell intrusion, is primarily a greenschist-facies mylonite zone separating the Southern Alps from the amphibolite facies units of the Central Alps (Lepontine dome), which were exhumed to shallow crustal levels till the Pliocene (e.g.,

Campani et al. 2010; Mahéo et al. 2013). The eastern sector, instead, runs north of the Adamello complex and separates it from the Austroalpine units, where the alpine overprint is confined to greenschist shear zones and cooling to temperatures ≥300 °C is Variscan (e.g., Viola et al. 2003). In this sector only 5 km of estimated north side up vertical displacement occurred during dextral strike-slip movement between 32 and 30 Ma (Schmid et al. 1996). Pure dextral strike-slip movement continued until ~20 Ma, after which the mylonites of the eastern Tonale fault were offset by sinistral shearing presumably due to activity along the Giudicarie fault (Stipp et al. 2002).

Giudicarie belt

The transpressive Giudicarie belt is a broad region of ESE-vergent thrusts and N–S trending sinistral strike-slip faults, bounded to the east by the sinistral Trento-Cles line and to the west by the sinistral transpressive Giudicarie line (Fig. 3), which are partially or totally the result of reactivation of Permian-Mesozoic normal faults (Castellarin et al. 1993; Picotti et al. 1995; Prosser 1998). The Giudicarie region was mainly affected by two phases of deformation during the Neogene: a Mid-Miocene phase, typified by the Valsugana thrust discussed below, and a younger, Late Miocene–Pliocene event, possibly associated with the initiation of the Montello–Friuli belt to the southeast (Caputo and Poli 2010; Castellarin and Cantelli 2000; Castellarin et al. 1992; Martin et al. 1998; Massironi et al. 2006; Viola et al. 2001).

The NNE-SSW-trending Giudicarie structural belt is oblique to the strike of the Southern Alps (Figs. 1, 3).

Along this belt there is evidence of a structural boundary at crustal scale (Spada et al. 2013), whose surface expressions are major differences between the sectors east and west of the Giudicarie belt. West of the Giudicarie belt south-vergent structures are sealed by the Early Oligocene Adamello complex (Figs. 1, 3) (Brack 1981), whereas to the east there is little pre-Adamello deformation (Bigi et al. 1990) limited to the Eocene Dinaric deformation from the Dolomites eastwards (Doglioni and Bosellini 1987). During the Miocene the south-vergent structures, both west and east of the Giudicarie belt, propagated into the Po Plain foreland. Subsequently, the deformed Miocene sediments to the west were partially or completely eroded or buried beneath younger sediments (Pieri and Groppi 1981) and the internal parts of the fold and thrust belt have undergone little to no recent deformation (D'Adda et al. 2011; Wolff et al. 2012). To the east, instead, the foreland sediments continued to be involved in the deformation throughout the Pliocene–Pleistocene (Venzo 1977; Massari et al. 1986). At present, the direction of maximum horizontal compressive stress derived from focal mechanism is roughly perpendicular to the thrust fronts along the Giudicarie belt compatible with its dextral strike-slip reactivation (Vigano et al. 2008).

Valsugana and Val Trompia thrusts

Two of the main structures of the Southern Alps are the Valsugana and Val Trompia thrusts that uplifted and exposed crystalline basement (Castellarin et al. 1988, 1993, Picotti et al. 1995) (Fig. 3). The timing of the deformation is well established along the Valsugana thrust, where AFT ages from the hanging wall of the thrust and detrital AFT data from the preserved syntectonic basin lying directly to the south constrain a period of intense activity between 12 and 8 Ma (Zattin et al. 2003, 2006). Clasts of Permian intrusives from the hanging wall appear in basin deposits by the Messinian, further arguing for intense uplift and erosion along the structure during the Late Miocene (Zattin et al. 2003).

The Val Trompia thrust borders the Adamello complex to the south, and it terminates to the east against the Giudicarie belt (Picotti et al. 1995) (Figs. 1, 3). It is part of a fold and thrust belt where AHe ages in both the footwall and hanging wall are within 1σ error indicating the fault has been inactive since the Mid-Miocene (Reverman et al. 2012).

Thermochronological methods

The methodology is briefly outlined here; details are given in a supplementary file. Fission tracks in apatite (AFT) are damage zones in the crystal lattice formed during the radioactive spontaneous fission of ^{238}U. At temperatures above ca. 110 °C tracks are annealed, whereas at temperatures below 60 °C tracks are retained. The range between these two temperatures is called the partial annealing zone (Carlson et al. 1999; Naeser 1979). AHe geochronology is based on the ingrowth of α-particles produced during the decay of U, Th and Sm. At temperatures exceeding 80 °C He is rapidly diffused and lost from the system, while at temperatures below 40 °C He is quantitatively retained (House et al. 2002; Wolf et al. 1996). The cooling rate, radiation damage and grain size control the temperature range for helium retention (Reiners and Farley 2001; Shuster and Farley 2009). AHe ages are corrected for He loss generated by α-ejection using a geometric correction factor (Ft). The total analytical error was computed as the relative standard error of weighted uncertainties on U, Th, Sm and He measurements. Ft corrections were made following Farley (2002).

The uncertainty of the age of a single-grain aliquot was calculated by the Gaussian error propagation from the U, Th, Sm and He measurements and from the estimated uncertainty of the Ft. The sample average is the unweighted arithmetic mean of the aliquot ages; the error is given as 2σ in the text and in Figs. 2 and 3. The scatter of the single-aliquot apparent ages derives mostly from submicroscopic inclusions, zoning of the alpha-emitting elements and from the differences between the sizes (diffusion domains) of the crystals (see, e.g., Fitzgerald et al. 2006). AHe analyses of the Austroalpine Karawanken samples were carried out in the Thermochronology Laboratory at Geoscience Center, University of Göttingen, Germany. The Southalpine samples were analyzed at the Noble Gas Lab, ETH Zürich.

Thermochronology results

Table 1 presents AHe results from the Karawanken Mountains, Table 2 the new AFT data and Table 3 AHe data from the Southern Alps. AHe ages range from 2.9 to 28.4 Ma, with a majority of samples falling between 6 and 12 Ma. AFT ages from the Southern Alps range from 7.9 to 29.7 Ma. The low number of spontaneous tracks in our samples prohibited the systematic measurement of confined track lengths, necessary for a detailed assessment of the thermal history. Below we discuss the ages in the context of each of the main structural features associated with the sampling. Errors are given as 2σ.

Karawanken Mountains

Samples for AHe analysis were taken from the gabbroic to granitic members of the Permian to Triassic North Karawanken plutonic and the Oligocene tonalitic southern

Table 1 (U–Th–Sm)/He analytical data from the eastern Periadriatic fault

Sample	Grain ID	Lithology	Location Lat (°N)	Long (°E)	Altitude (m)	He Vol. (ncc)	1σ	U238 Mass (ng)	1σ	Conc. (ppm)	Th232 Mass (ng)	1σ	Conc. (ppm)	Th/U ratio	Sm Mass (ng)	1σ	Conc. (ppm)	Ejection correct. (Ft)	Uncorr. He age (Ma)	Ft-Corr. He age (Ma)	2σ (Ma)	Sample unweighted aver. ± 1σ (Ma)
KA10	a1	Hbl-granite	46°28.480′	14°35.623′	581	0.078	2.6	0.058	2.1	40.8	0.143	2.5	100.0	2.45	0.498	6	347	0.66	6.7	10.1	1.2	
	a2					0.020	4.7	0.023	3.2	16.8	0.068	2.5	50.4	3.00	0.310	7	230	0.79	4.0	5.1	0.6	
	a3					0.034	3.3	0.031	2.7	19.2	0.053	2.6	32.3	1.68	0.379	7	231	0.64	6.1	9.5	1.3	8.2 2.7
KA16	a1	Tonalite	46°32.680′	13°50.737′	653	0.177	1.6	0.094	1.9	65.8	0.079	2.5	55.0	0.84	0.241	7	169	0.63	12.8	20.5	2.5	
	a2					0.209	1.5	0.105	1.9	51.2	0.128	2.5	62.0	1.21	0.398	7	194	0.61	12.5	20.3	2.5	20.4 0.1
KA17	a1	Granodiorite	46°28.492′	14°37.341′	655	0.023	4.1	0.024	3.2	17.3	0.054	2.5	39.3	2.27	0.202	8	147	0.65	5.0	7.7	1.1	
	a2					0.041	3.4	0.038	2.4	18.2	0.121	2.5	57.2	3.14	0.374	7	177	0.72	4.9	6.8	0.8	
	a3					0.092	2.4	0.101	1.9	39.8	0.115	2.5	45.1	1.13	0.548	7	215	0.77	5.8	7.4	0.7	7.3 0.4
KA18	a1	Diorite	46°28.621′	14°36.452′	619	0.063	2.6	0.070	2.0	31.7	0.159	2.4	72.0	2.27	0.905	6	410	0.67	4.6	6.8	0.8	
	a2					0.029	4.0	0.042	2.3	32.7	0.044	2.6	33.7	1.03	0.361	7	278	0.73	4.3	5.9	0.7	
	a3					0.078	2.4	0.081	2.0	33.9	0.146	2.5	61.3	1.81	0.847	7	356	0.63	5.3	8.4	1.1	7.1 1.3
KA19	a1	Gabbro	46°28.553′	14°35.318′	605	0.165	1.7	0.064	2.0	13.2	0.354	2.4	73.0	5.52	0.505	7	104	0.78	9.0	11.5	0.9	
	a2					0.220	1.8	0.087	1.9	24.6	0.369	2.4	104.0	4.23	0.441	7	124	0.82	10.2	12.4	0.9	
	a3					0.245	1.6	0.119	1.9	17.6	0.478	2.4	71.1	4.03	0.887	6	132	0.82	8.5	10.3	0.7	11.4 1.1
KA27	a1	Metabasite	46°28.857′	14°38.605′	706	0.007	7.7	0.005	14.5	4.3	0.029	2.7	25.4	5.96	0.292	8	254	0.54	3.9	7.3	1.7	
	a2					0.028	3.8	0.017	4.1	2.7	0.088	2.5	13.9	5.19	1.552	6	246	0.72	4.6	6.3	0.8	
	a3					0.014	5.5	0.011	6.5	3.4	0.046	2.6	14.1	4.09	0.890	6	270	0.74	3.9	5.3	0.8	6.3 1.0
KA7	a1	Tonalitegneis	46°27.967′	14°36.967′	645	0.162	1.8	0.110	1.9	18.7	0.219	2.4	37.2	1.99	0.999	6	169	0.77	7.9	10.2	0.8	
	a2					0.115	2.1	0.105	1.9	22.9	0.204	2.4	44.6	1.95	0.736	6	161	0.74	6.0	8.1	0.8	
	a3					0.170	1.7	0.129	1.9	21.7	0.236	2.4	39.6	1.83	1.046	6	175	0.75	7.3	9.6	0.8	9.3 1.1
KS14	a3	Tonalite	46°25.954′	14°58.373′	982	0.079	2.4	0.075	2.0	20.3	0.148	2.5	39.9	1.97	0.637	7	172	0.76	5.7	7.5	0.7	
	a4					0.070	2.4	0.089	1.9	33.0	0.059	2.5	21.7	0.66	0.454	7	168	0.66	5.4	8.2	1.0	
	a5					0.147	1.9	0.135	1.9	23.4	0.209	2.4	36.1	1.54	0.974	6	169	0.76	6.3	8.4	0.7	8.0 0.5
KS-11	a1	Tonalite	46°27.055′	14°49.973′	708	0.084	5.3	0.149	1.9	30.3	0.245	2.4	49.80	1.64	0.834	8.4	169.85	0.69	3.25	4.7	0.68	
	a2					0.152	2.7	0.154	1.9	21.4	0.241	2.4	33.48	1.57	1.040	8.4	144.65	0.76	5.73	7.5	0.71	
	a3					0.079	3.1	0.096	1.9	27.4	0.131	2.5	37.45	1.36	0.532	8.4	151.67	0.72	4.98	6.9	0.75	6.4 1.5
KAR-25	a2	Tonalite	N46°35.799′	E14°08.624′	800	0.138	2.9	0.039	2.4	5.5	0.026	2.7	3.7	0.68	0.518	8	73	0.80	23.1	28.9	2.7	
	a3					0.026	6.3	0.008	7.7	4.777	0.0	2.8	13.0	2.715	0.2	8.5	101.0	0.56	14.6	26.274	5.3	27.6 1.8

Table 2 AFT analytical data from the Southern Alps

Sample number	Long. (°E)	Lat. (°N)	Altitude (m)	No. of crystals	Spontaneous		Induced		Dosimeter		U (ppm)	$P(\chi)^2$	Age (Ma) $\pm 2\sigma$
					N_s	ρ_s	N_i	ρ_i	N_d	ρ_d			
VT2-10	10.3664	45.8446	2000	8	45	10.3	630	144	3658	114	16	64	14.5 ± 4.6
PBFT6	10.2185	45.8954	240	20	124	4.87	2211	86.8	3658	111	10	46	11.1 ± 2.2
PBFT8	10.1669	45.8820	280	20	98	10.1	1027	106	2859	110	12	84	18.9 ± 4.0
PBFT9	10.1659	45.8820	270	20	45	4.57	655	63.7	2859	107	7.4	92	13.8 ± 4.2
PBFT10	10.2810	45.9400	300	20	43	4.63	981	106	3658	102	13	53	7.9 ± 2.4
PBFT11	10.4157	45.8115	1990	20	91	9.09	574	57.4	2859	104	6.9	39	29.7 ± 7.0
PBFT12	10.6045	45.9473	600	20	68	7.68	1227	137	3658	110	16	3	11.3 ± 3.4
PBFT13	10.6045	45.9473	730	20	173	16.1	3476	323	3658	107	38	3.5	10.1 ± 2.2
BG72.2	10.4686	45.8185	640	20	57	4.65	806	65.8	3904	14.82	3.3	99	17.7 ± 4.9
VT1-10*	10.3783	45.8364	1935	20	177	26.4	3194	47.7	4454	143	40.7	86.9	9.9 ± 3.5
CDA1**	11.6051	46.1701	2130	19	58	8	1212	166	4910	103	20.6	97.8	9.1 ± 2.4
FRI**	11.2160	45.9677	1089	23	325	9.3	366	105	5924	125	5.1	39.4	202.5 ± 33.8

N_s: number of spontaneous tracks counted on internal mineral surface; ρ_s: spontaneous track density ($\times 10^4$ cm^{-2}); N_i: number of induced tracks counted on external mica detector; ρ_i: induced track density ($\times 10^4$ cm^{-2}); N_d: number of dosimeter tracks counted on external mica detector; ρ_d: dosimeter track density ($\times 10^4$ cm^{-2}); $P(\chi)^2$: probability of obtaining Chi-square value for n degrees of freedom (where n = number of crystals − 1); a probability >5 % is indicative of a homogenous population. AFT ages were obtained using the standard external detector method and the zeta calibration approach. The zeta value, obtained on Durango and Fish Canyon apatite standards (Hurford and Green 1983) for D. Seward is 360 ± 5, for R. Reverman (*) 257 ± 14, for M. Zattin (**) 346 ± 18. Ages given in this table and the text are central ages. Error is quoted as 2σ

belt along the eastern part of the PAF system and from the Paleozoic basement (Figs. 2b, 4; Table 1).

The α-ejection corrected mean AHe ages from within the positive flower structure of the Karawanken vary from 11 to 6 (±2) Ma without any systematic trends (Table 1). The most obvious change occurs outside the flower structure where AHe ages are substantially older. A site along the PAF but west of the flower structure and HMV fault yields an AHe age of 20 Ma (KA16) (Fig. 2b). A further AHe age of 28 ± 4 Ma (KAR25) was derived for the Oligocene Reifnitz tonalite north of the Karawanken Mountains, which is located in the basement of the Neogene Klagenfurt basin, in the footwall of the North Karawanken unit (Fig. 2b).

Tonale fault

Samples across the Tonale fault were taken as close as possible to previous AFT and ZFT samples but only a few locations provided suitable apatites for AHe dating. AHe ages across the Tonale fault record mostly Late Miocene cooling, though discrepancies occur (Figs. 3, 5). AHe ages north of the line are ~11 Ma (VST4 and VST5), while to the south ages at similar elevations show a larger spread between 6 and 12 Ma. Interestingly, ZFT analyses revealed a significant difference in cooling ages (Viola et al. 2003) with the oldest ages in the footwall of the Pejo fault (ca. 80 Ma), younger ages between the Pejo and Tonale faults

(ca. 50–20 Ma) and youngest ages south of the Tonale fault (Fig. 3). In contrast, AFT and our new AHe ages from samples in the same area do not show differential cooling (Figs. 3, 5) but imply Miocene cooling as a coherent block across the Tonale fault. A Pliocene (2.9 Ma, TL1) AHe age is found within the Austroalpine basement north of the line (Figs. 3, 5). Given that all other samples in the immediate area yield Miocene ages, we interpret this sample to have been recently reset (i.e., due to localized fluid flow), rather than indicating significant recent exhumation.

Valsugana thrust

AHe ages were obtained from samples that were previously dated by AFT analysis from the hanging wall of the Valsugana thrust (Zattin et al. 2003) (Figs. 3, 6, Section C). The highest elevation sample (CDA1) has AHe and AFT ages that are essentially the same, indicating rapid cooling at ~11 Ma, in agreement with previous studies (Zattin et al. 2003, 2006). While AFT ages are invariant at lower elevations, the AHe ages get slightly younger (~7 Ma). Two AHe ages were obtained on samples from basement highs that were never buried by more than 4 km of sediments since the Cretaceous (Bosellini and Doglioni 1986) (Fig. 3). These samples (FRI and CAL11) yield Oligocene AHe (27 and 28 Ma) and Mesozoic AFT ages (77 and 202 Ma). In sample FRI two grains (a1 and a4) yield anomalously older ages and the remaining two grains yield Oligocene ages

Table 3 (U–Th–Sm)/He analytical data from the Southern Alps

Sample	Grain ID	Lithology	Long (°E)	Lat (°N)	Altitude (m)	Mass (µg)	4He (fmol)	238U (fmol)	232Th (fmol)	147Sm (fmol)	eU (ppm)	Uncorr. He age (Ma)	Analytical error (Ma)	Ejection correct. (Ft)	Ft-Corr. He age (Ma)	Mean age (Ma)	σ (Ma)
Tonale fault (S)																	
VS13	a1	Tonalite, Pre-sanella unit	10.6556	46.2556	1935	2.86	2.13	298.49	359.44	467.18	35.18	4.30	0.06	0.71	6.03	6.7	0.6
	a2					1.87	2.35	313.08	361.35	429.38	55.78	4.57	0.07	0.68	6.72		
	a3					2.29	1.97	239.57	298.48	421.77	35.67	4.90	0.08	0.68	7.24		
VS4	a2	Tonalite, Pre-sanella unit	10.6393	46.2275	2916	1.52	2.03	178.64	289.13	297.62	43.71	6.37	0.11	0.65	9.86	9.8	0.1
	a3					2.11	2.51	215.98	313.81	431.67	36.58	6.69	0.10	0.69	9.67		
VS11	a3	Tonalite, Pre-sanella unit	10.6565	46.2429	2300	1.42	1.53	183.76	195.84	227.66	42.12	5.14	0.10	0.65	7.89	8.5	1.1
	a2					5.11	6.56	669.20	819.63	1138.40	44.42	5.89	0.07	0.76	7.77		
	a1					2.23	3.34	363.68	81.04	233.24	42.04	6.75	0.09	0.70	9.71		
VS7	a3	Tonalite, Pre-sanella unit	10.6431	46.2316	2703	4.61	5.83	414.27	716.61	903.06	34.14	7.73	0.09	0.74	10.45	11.6	1.2
	a2					4.73	4.81	320.32	277.10	474.96	20.99	9.64	0.11	0.75	12.86		
	a1					4.60	7.94	514.08	832.86	1024.97	41.51	8.65	0.10	0.75	11.60		
Fault zone																	
VS3	a1	Schist, Tonale unit	10.6553	46.2744	1362	5.31	0.26	13.04	145.73	74.24	2.82	4.36	0.21	0.76	5.72	8.3	3.8
	a2					3.89	0.39	44.26	74.13	134.25	4.27	4.93	0.17	0.75	6.56		
	a3					3.59	0.34	9.15	80.35	50.81	2.43	9.32	0.32	0.73	12.72		
DIM1	a1	Tonalite, Pre-sanella unit	10.8650	46.3202	850	3.80	32.38	145.46	2756.35	475.00	48.67	32.05	1.15	0.71	45.09	6.4	0.8
	a2					2.24	6.55	768.46	1669.20	579.30	122.93	4.39	0.08	0.66	6.62		
	a3					2.68	7.69	842.78	1604.24	473.47	108.03	4.91	0.08	0.69	7.08		
	a4					2.24	2.62	418.89	540.82	231.68	58.02	3.73	0.07	0.67	5.58		
Tonale fault (N)																	
TL1	a1	Schist, Tonale unit	10.6677	46.2881	1376	15.97	6.90	1690.26	22.28	2251.55	25.49	3.13	0.04	0.83	3.76	2.9	0.8
	a2					46.16	6.46	2506.07	135.16	2795.57	13.25	1.96	0.02	0.88	2.24		
	a3					7.48	1.27	458.49	5.10	581.37	14.74	2.13	0.04	0.78	2.71		
VST4	a1	Schist, Tonale unit	10.6062	46.2960	2276	1.17	0.63	56.63	3.89	57.58	11.84	8.46	0.24	0.64	13.28	10.8	2.1
	a2					11.51	8.61	753.25	50.19	599.49	16.05	8.68	0.11	0.83	10.42		
	a3					10.48	0.53	43.77	b.d.	209.95	0.99	9.26	0.22	0.83	11.17		
	a4					1.61	0.20	27.61	b.d.	37.29	4.06	5.52	0.37	0.68	8.17		
VST 5	a1	Schist, Tonale unit	10.6375	46.2792	1624	5.30	10.98	951.52	173.88	1379.23	44.82	8.51	0.10	0.78	10.89	11.3	0.5
	a2					4.68	11.68	1039.44	149.75	1237.88	54.96	8.37	0.10	0.75	11.18		
	a3					6.20	15.60	1256.30	189.61	1501.70	50.22	9.24	0.11	0.78	11.82		
	a4																

Table 3 continued

Sample	Grain ID	Lithology	Long (°E)	Lat (°N)	Altitude (m)	Mass (μg)	4He (fmol)	238U (fmol)	232Th (fmol)	147Sm (fmol)	eU (ppm)	Uncorr. He age (Ma)	Analytical error (Ma)	Ejection correct. (Ft)	Ft-Corr. He age (Ma)	Mean age (Ma)	σ (Ma)
Giudicarie belt																	
01RZ12	a1	Eocene, Ponte Pia Fm	10.9726	46.1307	1023	20.52	25.90	1532.75	3700.64	3234.05	27.75	8.35	0.09	0.84	9.94	10.4	0.6
	a2					5.98	7.11	472.32	719.57	773.48	25.51	8.58	0.12	0.77	11.16		
	a3					1.62	1.82	126.90	363.92	308.44	30.99	6.64	0.13	0.65	10.24		
02RZ12	a1	Eocene, Ponte Pia Fm	10.9761	46.1307	1023	4.73	4.85	298.03	773.99	750.73	24.00	7.82	0.11	0.75	10.43	9.9	0.5
	a2					6.03	7.14	454.71	1214.65	925.29	29.08	7.48	0.09	0.77	9.76		
	a3					4.60	5.14	361.08	861.52	757.27	29.01	7.06	0.10	0.75	9.44		
05RZ12	a1	Eocene, Ponte Pia Fm	11.0653	46.2723	332	9.57	33.44	1027.03	2469.96	952.81	39.79	16.17	0.18	0.79	20.51	17.0	3.3
	a2					10.62	31.38	1040.17	3448.75	1264.08	41.18	13.20	0.15	0.80	16.56		
	a3					4.63	9.71	407.81	1364.50	508.90	37.19	10.38	0.13	0.74	14.04		
vd 11	a1	Tonalite, Western Adamello unit	10.5644	46.0859	1908	3.16	4.50	418.12	689.39	737.49	43.62	6.00	0.08	0.72	8.35	7.9	0.6
	a2					2.40	2.51	291.39	449.86	513.95	39.31	4.89	0.08	0.67	7.27		
	a3					6.63	7.72	693.18	1150.45	1346.53	34.53	6.20	0.08	0.76	8.21		
VM5-10	a1	Tonalite, Western Adamello unit	10.4713	46.1278	2522	8.99	8.26	973.46	1569.69	1804.27	35.47	4.76	0.06	0.79	6.02	5.9	0.1
	a2					1.98	2.14	309.70	506.95	492.90	51.37	3.86	0.07	0.66	5.85		
	a3					2.86	3.09	422.43	672.11	652.42	48.22	4.12	0.07	0.71	5.85		
VM6-10	a1	Tonalite, Western Adamello unit	10.4420	46.1306	2070	7.01	7.82	863.04	90.33	813.56	30.21	6.82	0.10	0.77	8.80	7.8	1.0
	a2					3.91	5.13	201.54	270.14	231.38	16.13	14.99	0.31	0.73	20.62		
	a4					2.06	2.21	299.94	284.29	241.77	42.42	4.67	0.07	0.68	6.85		
	a5					4.37	5.36	584.63	586.77	498.40	39.43	5.75	0.08	0.76	7.60		
Valsugana																	
CDA1	a1	Cima D'Asta granite	11.6051	46.1701	2480	1.19	1.03	154.64	336.14	794.26	46.56	3.39	0.07	0.57	5.90	9.5	3.2
	a2					1.58	2.79	239.39	328.61	472.20	47.75	6.77	0.13	0.64	10.57		
	a3					0.92	1.03	76.34	182.81	442.09	30.86	6.61	0.19	0.55	11.99		
CAL1	a1	Cima D'Asta granite	11.4955	46.0876	722	4.54	4.86	574.34	858.45	1384.39	40.68	4.83	0.07	0.74	6.53	6.9	0.3
	a2					1.68	1.70	228.36	283.57	494.99	41.86	4.44	0.10	0.63	7.05		
	a3					1.35	1.35	184.12	193.63	356.27	40.67	4.52	0.11	0.64	7.07		
CAL11	a4	Paragneiss	11.2985	46.0514	1640	3.19	4.52	79.34	219.64	551.61	9.71	26.33	0.40	0.71	36.94	28.4	8.5
	a2					7.27	12.31	359.93	1090.09	2633.63	20.05	15.27	0.20	0.77	19.87		
	a1					4.04	7.08	158.26	464.34	1553.48	15.65	20.07	0.30	0.71	28.35		

Table 3 continued

Sample	Grain ID	Lithology	Long (°E)	Lat (°N)	Altitude (m)	Mass (µg)	4He (fmol)	238U (fmol)	232Th (fmol)	147Sm (fmol)	eU (ppm)	Uncorr. He age (Ma)	Analytical error (Ma)	Ejection correct. (Ft)	Ft-Corr. He age (Ma)	Mean age (Ma)	σ (Ma)
CAL2	a5	Cima D'Asta granite	11.5009	46.0966	875	2.75	5.73	721.42	628.22	926.00	75.32	5.10	0.07	0.70	7.25	9.0	2.3
	a6					1.96	3.76	318.12	199.45	368.61	44.36	7.95	0.11	0.68	11.64		
	a4					2.01	4.88	575.03	572.45	904.85	84.23	5.32	0.12	0.66	8.04		
FRI	a1*	Paragneiss	11.2160	45.9677	1089	1.42	81.92	73.26	346.66	1010.41	25.64	392.46	5.90	0.58	678.15	27.2	4.5
	a2					1.78	6.28	141.14	413.33	1075.33	31.68	20.10	0.27	0.66	30.44		
	a3					1.11	2.45	71.31	259.30	794.13	28.19	14.04	0.26	0.58	24.01		
	a4*					1.56	11.66	86.05	324.98	1185.22	24.60	53.96	0.74	0.66	82.33		
Val Trompia-Val Camonica																	
PBFT6	a1	Permian, Auccia Volcanics	10.2185	45.8954	240	1.22	0.31	38.01	76.75	394.17	10.90	4.13	0.18	0.61	6.73	7.0	0.4
	a2					3.90	2.36	226.52	437.14	1408.81	20.04	5.46	0.07	0.75	7.30		
	a3*					1.68	0.79	37.15	104.41	497.14	8.71	9.55	0.23	0.66	14.37		
	a4*					1.75	2.79	91.50	83.53	227.10	15.16	19.31	0.27	0.69	28.01		

* Grain rejected from age calculation (see text for details)
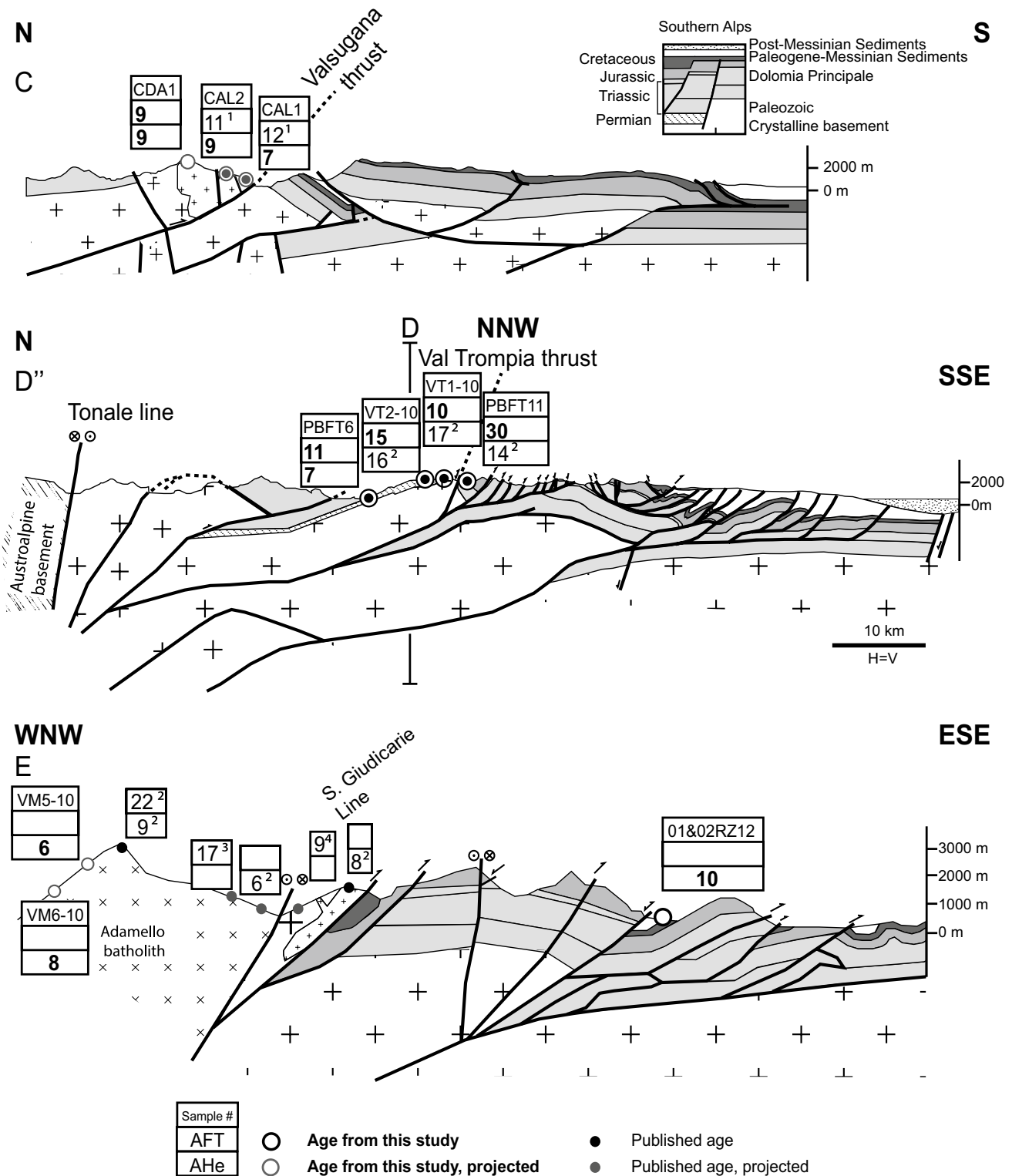
Fig. 6 Cross sections of the central Southern Alps. *Section C*: N–S cross section of the Valsugana thrust. Published ages are from [1]Zattin et al. ([2003]). Cross section modified after Caputo and Bosellini ([1994]), Selli ([1998]) and Barbieri and Grandesso ([2007]). *Section D* and *D″*: N–S and NNW–SSE cross section of the Val Trompia thrust. Published ages are from [2]Reverman et al. ([2012]). Cross section modified after Schoenborn ([1992]) and Picotti et al. ([1995]). *Section E*: Ca. W–E cross section of the Giudicarie belt. Published ages are from [2]Reverman et al. 2012; [3]Viola 2000, [4]Viola et al. 2001. Cross section after Picotti et al. 1995. Traces of the sections are indicated in Fig. 3

similar to those found in sample CAL11 (Table 1). Both samples have a high dispersion of individual grain ages, which suggests, along with the relatively large discrepancy with their AFT ages, very slow cooling since the Mesozoic.

Val Trompia thrust

We present ten new AFT ages and one new AHe age from the Val Trompia area (Figs. 3, 6, Section D″/D). All ages record Middle to Late Miocene cooling. The AFT data show a discrepancy in ages across the fault, with 29.7 Ma (PBFT11) in the footwall and 14.5 Ma (VT2-10) and 9.9 Ma (VT1-10) in the hanging wall. However, no major discrepancies in the AHe ages occur across the fault, where the ages from the hanging wall are slightly older, but within error, of those in the footwall, 16.4 and 13.5 Ma, respectively (Reverman et al. 2012).

A noticeable problem in the hanging wall is that the AFT ages are younger than the AHe ages. Inversion of AFT and AHe ages has been identified in several studies and has yet to be fully explained, though it is often argued that the problem lies either in zonation of the parent nuclides, or He implantation from neighboring grains with high U content, or in an imperfect understanding of helium diffusion kinetics for samples with complex and slow cooling histories (Ault and Flowers 2012; Flowers et al. 2009; Green and Duddy 2006; Shuster et al. 2006; Spiegel et al. 2009), all of which are applicable to these samples.

Giudicarie belt

In the Giudicarie belt samples were collected with the aim of quantifying vertical offsets across this major boundary. However, suitable apatite bearing lithologies are scarce. Three samples were taken from the Ponte Pià formation, reworked intermediate tuffs of the Eocene Giudicarie-Insubric Flysch (Castellarin et al. 1993, 2006; Sciunnach 1994) (Figs. 2, 6, Section E). The northern sample (05RZ12) records an AHe age of 17 Ma, while the two southern samples (01RZ12 and 02RZ12) yield ages of ~10 Ma.

Discussion

In the following, we will first discuss evidence for Late Miocene exhumation along the eastern PAF segment in the Karawanken Mountains, then discuss late-stage cooling in the Southern Alps, followed by a synthesis of evidence for widespread latest Mid-Miocene to Late Miocene foci of deformation and exhumation. We will proceed with a discussion of the potential engine driving Late Miocene

exhumation in the frame of the broader Neoalpine evolution and Adriatic indentation.

Late-stage exhumation at the leading edge of the indenter in the Karawanken Mountains

Our new AHe cooling ages ranging from 13 to 4 Ma from the Karawanken flower structure in conjunction with the clastic record from the Klagenfurt basin (Nemes et al. 1997 and references therein) indicate a hitherto undated late Neogene exhumation pulse along the eastern segment of the PAF. This pulse was associated with surface uplift and topography growth during the formation of the flower structure and thrusting of the North Karawanken unit onto proximal clastic deposits of the Klagenfurt basin, the only flexural basin inside the Alps. The coarsening-upward sequence of the basin fill derived from the Karawanken clearly reveals the initiation of uplift and fast-growing relief of the chain (Polinski and Eisbacher 1992 and references therein). Further evidence for rapid cooling comes from an AFT age of 12.8 ± 1.8 (Nemes 1996) from the Karawanken tonalite (Fig. 2b). This age is only slightly older than the AHe ages presented herein, suggesting rapid upper crustal cooling and unroofing on the order of 3–5 km since latest Mid-Miocene time.

Importantly, AHe ages derived from outside the Karawanken flower structure are distinctly older: Along the western segment of the eastern PAF, no similar Late Neogene shortening occurred, as evidenced by an older AHe age of 20 Ma (KA16) from west of the Hochstuhl–Möll Valley fault system (Fig. 2b). Combining our new age with published AFT ages of 26 ± 2 Ma from the same locality and 25 ± 2 Ma further west (Hejl 1997) attests to an earlier phase of Late Oligocene to Early Miocene cooling. A further AHe age of 28 ± 4 Ma from the Reifnitz tonalite (KAR25) corroborates that Late Miocene cooling has not seriously affected the Austroalpine lid from the immediate surroundings of the Karawanken flower structure.

An earlier cooling phase may be related to Late Oligocene to earliest Miocene NNW-ward advancement of the eastern Adriatic indenter (Pomella et al. 2011, 2012), and possibly its incipient northward subduction (Handy et al. 2014; Lippitsch et al. 2003) leading to a phase of major extrusion, mainly in the Tauern Window. In its western part rapid exhumation (2–4 mm/a) was bracketed between 20 and 12–10 Ma (Fügenschuh et al. 1997). During this early extrusion phase strain concentration in front of the tip of the indenter within the Tauern Window was influenced primarily by the occurrence of wedge-shaped blocks of Austroalpine units at the leading edge of the eastern Adriatic indenter (Scharf et al. 2013). These blocks may have

undergone internal fragmentation into the Drau–Möll and Rieserferner blocks (Fig. 2a) at the end of the Oligocene triggering ESE-ward migration of exhumation in the Eastern Tauern subdome (Favaro et al. 2015).

Late-stage exhumation in the Southern Alps

Throughout most of the Southern Alps exhumation of deep crustal material did not occur and erosion of less than 10 km is evident from the Mesozoic ZFT ages and the Mesozoic-to-Eocene AFT ages recorded in the Orobic Alps (Bertotti et al. 1999; Zanchetta et al. 2011, 2015), the Giudicarie region (Zattin et al. 2006) and the Dolomites (Emmerich et al. 2005). Shortening during Alpine orogeny led to significant exhumation mainly in localized areas in and around the Giudicarie belt. We find Late Miocene ages (AFT and AHe) as a first-order feature of the cooling and exhumation pattern of the central-eastern Southern Alps. Major Late Miocene exhumation along the Valsugana thrust, already indicated by Tortonian AFT ages from the Valsugana thrust (Zattin et al. 2006) and its southern foreland (Monegato and Stefani 2010), is corroborated by our new AHe data. Unroofing of ca. 4 km of sediment along the thrust and exposure of the crystalline basement correlates with rapid growth, migration and erosion of the Southalpine fold-and-thrust belt. AFT ages to the north and immediately to the west of the Valsugana thrust (e.g., CAL11 77.4 Ma, Fig. 2) are Mesozoic (Emmerich et al. 2005; Zattin et al. 2003) indicating that Miocene exhumation was limited to and focused along the fault. Moreover, the Oligocene AHe ages in the western sector of the Valsugana thrust indicate differential amounts of exhumation along this structure, which cannot be explained simply by differential thickness of Mesozoic sediments due to inherited structural highs and lows (Bosellini and Doglioni 1986). This pattern of focused exhumation can be extended to the Val Trompia fault, where Middle to Late Miocene AFT ages are found juxtaposed with Oligocene ages across the fault (Fig. 6, Section D″/D).

The Late Miocene ages found in the Giudicarie belt and Adamello area are ascribed to uplift associated with basement ramps that folded the earlier/older thrust sheets in the area (Fig. 6, Section D″/D) during thickening of the wedge. The uplift of the entire Adamello complex likely occurred due to it acting as a rigid block, whereas elsewhere in the Southern Alps an inherited network of Mesozoic faults allowed for strain partitioning and localization of deformation. A similar Tortonian pulse of exhumation has also been reported for the northern sectors of the central Southern Alps based on AFT data (Zanchetta et al. 2015).

Along the Giudicarie belt, the Miocene AHe ages from Eocene sedimentary units (Ponte Pia Fm) indicate that locally significant erosion affected not only the deepest units of the Southern Alps along the main thrusts but locally also the top of the sedimentary pile with removal of up to 2 km of overburden between deposition and the Mid- to Late Miocene, when exhumation occurred. The overburden of the Eocene units located in the core of the Giudicarie belt could have been partly due to thrusting (samples 01RZ12 and 02RZ12) as suggested by their location between imbricated thrust sheets and their AHe age of 10 Ma (Fig. 6, Section E). Nevertheless for the sample from the Eocene units with an AHe age of 17 Ma (05RZ12) located to the east of the Trento-Cles fault, there is no unequivocal evidence of overthrusting suggesting that the nature of the overburden there could have been sedimentary. The 2-km estimate of sedimentary overburden is well in line with vitrinite reflectance and solid bitumen reflectance measurements from the Dolomites indicating about 1800 ± 200 m of eroded thickness (Grobe et al. 2015) as well as the preservation of Oligocene/Miocene coastal sediments at ca. 2600 m altitude in the Eastern Dolomites (Keim and Stingl 2000). Moreover, the location of the older sample supports the argument for a general southward advance of deformation for the eastern Southern Alps (Mellere et al. 2000; Zattin et al. 2006). This argument is based on the structural evolution of the belt and of its foreland basin. In fact, an increase in subsidence in the Venetian Friuli basin is also recorded at 17 Ma (Mellere et al. 2000), while maximum subsidence occurred from the Serravallian to the Messinian in relation to tectonic loading due to the advancing Southalpine thrust belt. Given the petrologic evolution upsection of the foreland basin sediments, from carbonates (Cretaceous-Jurassic), to dolomites (Triassic), to metamorphic and volcanics (Permian), rapid progressive unroofing of the Southalpine basement must have occurred during the Serravallian to Messinian (Massari et al. 1986; Mellere et al. 2000; Zattin et al. 2003). The timing of basin subsidence and aggradation fits well with our results about the overall timing of exhumation in the Southern Alps and suggested geodynamic models (Bressan et al. 1998; Massironi et al. 2006).

In summary, major S-directed thrusting and rapid growth of the Southalpine fold-and-thrust belt within the eastern Adriatic indenter was active during the Serravallian (Castellarin and Cantelli 2000) or the Tortonian (e.g., Doglioni and Bosellini 1987; Schoenborn 1992), corroborated by thermochronological data evidencing Mid-Late Miocene exhumation. Accordingly, the eastern Adriatic indenter must have behaved in a rather rigid manner for ca. 8 myr with only little internal deformation in its northernmost sector (Caputo and Poli 2010 and references therein) after initial indentation at ca. 21 Ma. In "Driving forces for Late Miocene deformation and exhumation" section we will discuss in more detail how and why strain was accommodated differently in response to indentation.

Further evidence for late-stage exhumation

Our new thermochronological data from the Southern Alps and the Karawanken Mountains clearly indicate that latest Middle to Late Miocene unroofing is a widespread phenomenon at the leading and the western edge as well as within the eastern Adriatic indenter. Further evidence for NNW–SSE shortening and related exhumation exists at the northeastern edge of the indenter: east of the Lavant fault vitrinite reflectance and AFT data (10–14 Ma) from the northern Sava fold (Fig. 1) (Boc anticline) indicate Late Miocene shortening, basin inversion and exhumation on the order of 2.5–3 km south of the PAF (Sachsenhofer et al. 2001; Tomljenović and Csontos 2001). Folded latest Early and Middle Miocene rocks east of the Lavant fault also suggest that pronounced dextral transpression and deformation occurred during the Late Miocene (Fodor et al. 1998). According to these authors, dextral transpression along the Slovenian part of the PAF system culminated during the Late Miocene, in line with the evolution of the Karawanken flower structure. Evidence for yet younger, Plio-Pleistocene activity of the PAF system and the Sava fault associated with uplift of the Slovenian Kamnik Mountains has recently been shown in a study on cave sediments (Häuselmann et al. 2015). This might indicate a migration of Late Miocene exhumation from the North Karawanken Mts. southward into the Kamnik Mts. during Pliocene times during ongoing or renewed transpression.

As outlined above ("Late-stage exhumation at the leading edge of the indenter in the Karawanken Mountains" section) the push of the eastern Adriatic indenter initiated rapid exhumation within the Tauern Window in the Early Miocene (Foeken et al. 2007; Fügenschuh et al. 1997; Scharf et al. 2013). Processes related to indentation persisted throughout the Miocene and may be ongoing today (e.g., Caporali et al. 2013; Massironi et al. 2006), but their rates slowed down during Middle to Late Miocene time (e.g., Fügenschuh et al. 1997; Schneider et al. 2015). Based on thermochronology data from tunnel and surface samples from the Penninic Hochalm-Ankogel dome, that yielded slightly older AFT and AHe ages than those reported here (Figs. 2, 4), Foeken et al. (2007) suggested that the present-day topography evolved between 10 and 7 Ma during a phase of slow cooling (2–4 °C/Ma), after the major exhumation phase (ca. 22-16 Ma) associated with rapid cooling (40 °C/Ma). This Late Miocene phase of relief evolution in the SE Tauern Window is in line with palinspastic restorations that denote a Late Miocene age to the evolution of the Eastern Alps topography into a more mountainous landscape and a switch from a N–S-directed to a W–E-directed drainage system (Brügel et al. 2003; Frisch et al. 1998; Robl et al. 2008).

The Hochstuhl–Möll Valley fault system delimits the North Karawanken block to the west and shortening by thrusting disappears within a few kilometers, as also evidenced by narrowing of the westernmost Klagenfurt basin. W of the Hochstuhl fault, the basin fill is composed of about 150 m of gently folded Neogene strata, which die out laterally after a few kilometers, as well as a few tens of meters of Quaternary deposits. In contrast, to the east of the fault more than 600 m of flat-lying Tertiary clastics are overlain by up to 150 m of Quaternary deposits (Polinski and Eisbacher 1992). No flower structure nor thrust fault is known further west along the Pusteria–Gailtal fault though a subvertical ductile strike-slip duplex (Eder unit) with Early Oligocene cooling ages has been reported from the Carnian Alps (Läufer et al. 1997).

The young ages reported here contrast with Paleogene AHe ages from Austroalpine units east of the Tauern Window (Wölfler et al. 2011) (Fig. 2a). There, hilly and moderately shaped remnants of Miocene planation surfaces are widespread ("cold spots" according to Hejl 1997) as opposed to the steep relief, at places in excess of 1500 m of the Karawanken Mts. and the Tauern window, without such paleosurfaces. This part of the Eastern Alps has experienced significantly less postcollisional shortening and exhumation and no upright folding in contrast to the Tauern Window with high-amplitude folding, major exhumation and erosion (e.g., Rosenberg et al. 2015). Our AHe data in conjunction with published age constraints allow one to construct an improved pattern of spatial heterogeneity of exhumation of the Austroalpine unit, which is more complex than previously thought. Distinct blocks in the Eastern Alps and northernmost Dinarides experienced a Late Miocene widely distributed deformation phase accompanied by significant rock uplift (Fig. 7).

Wrench deformation along the eastern PAF system reveals a peculiar pattern of strain localization/concentration: Strain was accommodated over a wide area in the SE Alps and NE Dinarides between Medvenica Mts./Karlovac basin (van Gelder et al. 2015) and the PAF system south of the Pohorje Mts. (Sava folds) (Fig. 1). In contrast, in the Karawanken Mountains, strain localization was most efficient and strain was concentrated within the narrow belt of the flower structure, with mainly NW thrusting and formation of the flexural Klagenfurt basin (Nemes et al. 1997).

We attribute different deformation styles to contrasting preceeding thermal evolution and resulting lateral differences in crustal strengths: Pervasive Sava folding resulted from thermal crustal weakening due to addition of heat during syncollisional Early Miocene magmatism and extreme extension in the Early-Middle Miocene (Sachsenhofer et al. 2001; Fodor et al. 2008 and references therein) (Fig. 7). Weak lithosphere has also been reported for the Tauern
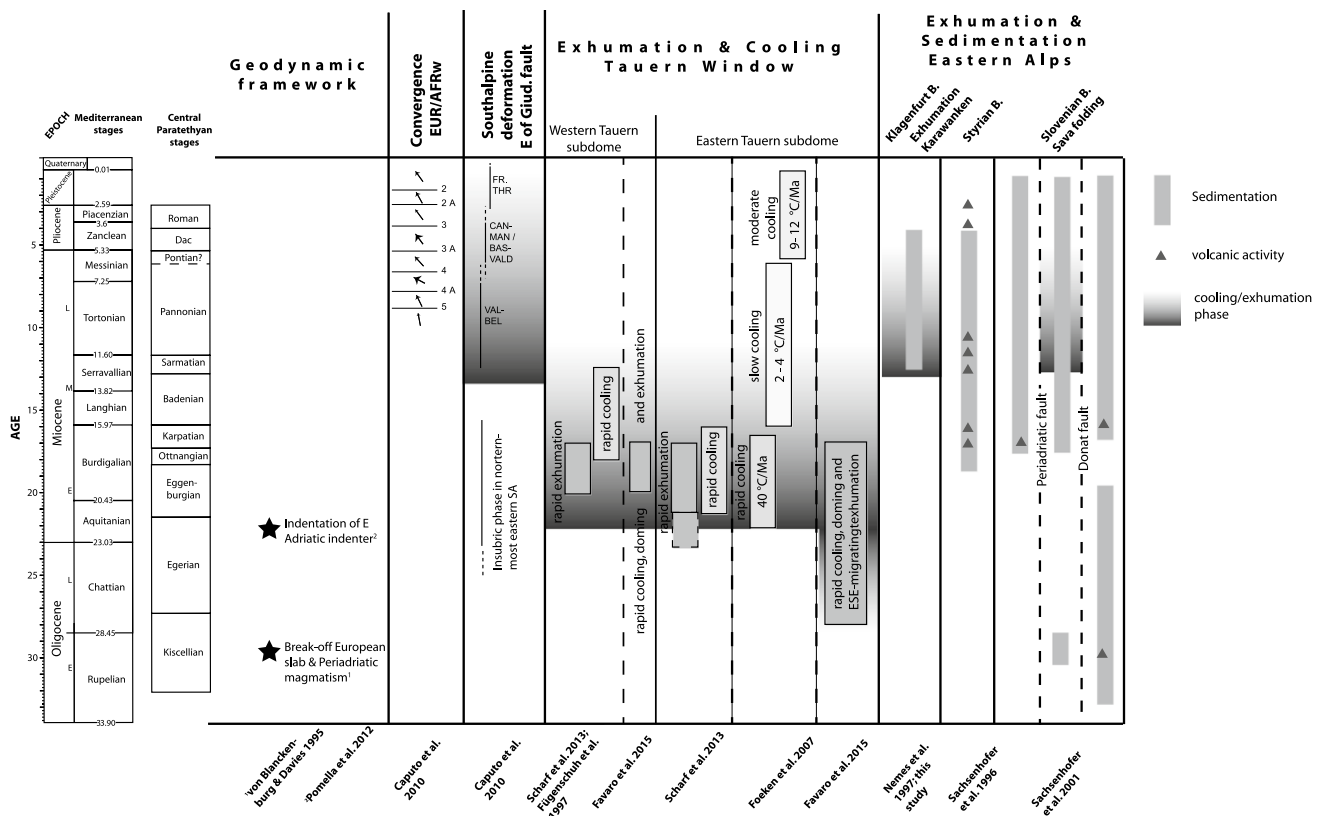
Fig. 7 Summary of episodes of major deformation, cooling, exhumation as well as sedimentation and volcanic activity for the Eastern and Southern Alps. Chronostratigraphic correlation chart for the Mediterranean and Paratethyan stages according to Piller et al. (2007). South-

alpine thrust systems: *VAL-BEL* Valsugana and Belluno, *CAN-MAN* Cansiglio-Maniago, *BAS-VALD* Bassano-Valdobbiadene, *FR. THR* frontal thrusts

Window (Genser et al. 2007; Willingshofer and Cloetingh 2003 and references therein), where northward movement of the eastern Adriatic indenter was initially accommodated by major ductile folding, exhumation and erosion as well as lateral extrusion. In contrast, such folding did not occur in the Karawanken Mountains and in the Southern Alps. Here mechanically stronger crust, which had experienced only weak Alpine metamorphic overprint, may have promoted localized strain concentration along faults (Karawanken flower structure; Valsugana thrust) instead.

Driving forces for Late Miocene deformation and exhumation

Based on our new low-temperature thermochronology ages and published data we observe a shift of strain distribution during the Miocene. Early Miocene exhumation is clearly focused within the Tauern Window in front of the Eastern Adriatic indenter and the wedge-shaped Austroalpine blocks (Rieserferner and Drau-Möll blocks in Fig. 2a) (e.g., Fügenschuh et al. 1997; Scharf et al. 2013) (Fig. 7). Late Miocene exhumation is, however, more distributed, but also

of smaller magnitude, indicating that convergence between the eastern Adriatic indenter and Europe is less focused and thus accommodated differently. Based on brittle fault analyses yielding predominant extensional and strike-slip states of stress in the Tauern Window, Bertrand et al. (2015) argued for such a switch in accommodation mechanism with initial vertical extension followed by strike-slip and normal faulting under constant N–S compression. This shift was triggered after orogen-scale folds were nearly isoclinal and the push of the indenter needed to be accommodated differently, leading to normal faulting and E–W extension within the Tauern Window. Importantly, this second stage initiated in the Late Miocene (Bertrand et al. 2015), coeval with more widespread exhumation in the Southern and Eastern Alps outlined above.

A possible mechanism leading to the observed exhumation pattern may lie in a shift of the mechanical coupling state and rheological behavior between the orogenic wedge and adjacent plates. Based on lithosphere-scale analogue modeling, Willingshofer and Sokoutis (2009) demonstrated that coupling is a key process for stress transmission and thus for the resulting deformation pattern. The amount of

coupling will increase during continental collision following subduction. They correlated their experimental results with the pattern of deformation in the Eastern Alps and observe a switch from north-directed to south-directed thrusting as well as initiation of internal deformation of the indenter between ca. 12 and 10 Ma. Based on numerical modeling Robl and Stüwe (2005) argue for a strong decrease in rheology contrast between the initially much stiffer Adriatic indenter into the softer European margin. Interestingly, substantial strengthening of the indented Eastern Alpine orogenic wedge occurred since ca. 13 Ma (Robl and Stüwe 2005). These modeling results are well in line with our findings of a latest Mid- to Late Miocene shift from focused exhumation outside of the indenter (mainly Tauern Window) to more widespread exhumation within and along the rims of the indenter (Fig. 7). Major coupling of the Alpine wedge and the South Alpine fold and thrust belt is also evidenced by the fault framework and fault linkages between the Austroalpine and Southalpine domains, which were fully developed during the latest Miocene–early Pliocene (Bartel et al. 2014a, b; Massironi et al. 2006).

A further plausible mechanism may have been a reorganization of the stress field leading to a change in boundary conditions operating on the orogen. Neogene convergence rates based on shortening values are 0.6–1 cm/year (Rosenberg and Berger 2009). However, magnetic anomalies and structural analyses indicate a change in relative plate motion of Africa with respect to Europe from NE to NNW 16 Ma ago and from NNW to NW 8.5 Ma ago (Caputo and Poli 2010 and references therein). Such rotations may have governed the compressional stress field in the study area and may have intensified strain transfer and exhumation.

In summary, we suggest that a major change of the coupling state of the orogen, possibly enhanced by a reorganization of the large-scale stress field between Africa and Europe initiated widespread latest Mid- to Late Miocene deformation, thrusting and exhumation at various sites within, at the rim and at the tip of the indenter.

Young uplift in the Eastern Alps?

Triggered by the detection of a dramatic increase in sediment flux to circum-Alpine basins since ca. 5 Ma (Kuhlemann et al. 2002) a large number of studies focused on the question, whether there has been a coeval, possibly climatically triggered increase in exhumation and erosion (e.g., Cederbom et al. 2004; Willett et al. 2006). In situ as well as detrital thermochronological data challenge sediment budget calculations and instead imply earlier phases of rapid exhumation or long-term steady-state conditions for the Western and Central Alps (e.g., Bernet et al. 2009;

Glotzbach et al. 2011; Fox et al. 2015). Only few studies have addressed this point for the Eastern Alps (Wölfler et al. 2012), which are tectonically more active than the Western and Central Alps, where convergence stopped at ca. 6 Ma (Battaglia et al. 2004; Grenerczy et al. 2005). In the Eastern Alps, an increasing body of data is testifying to a yet younger stage of uplift and/or erosion (e.g., Wagner et al. 2010). Genser et al. (2007) report late-stage surface uplift of the eastern Molasse basin on the order of 400 m since ca. 6 Ma. Gusterhuber et al. (2012) find evidence for even more intense erosion of 1–2 km of the Alpine foreland basin since Late Miocene times. Pliocene-Quaternary uplift also occurred in the Styrian basin (Sachsenhofer et al. 1997), the western part of the Pannonian basin (Bada et al. 2001) and the easternmost unglaciated part of the Eastern Alps (Legrain et al. 2014, 2015; Wagner et al. 2010) (Figs. 1, 2). The cause of this uplift is controversially debated, being associated with either (1) crustal delamination and/or convective removal of thickened lithosphere (e.g., Genser et al. 2007), (2) the coeval major reorganization of the external stress field in the ALCAPA region (e.g., Horváth and Cloetingh 1996; Peresson and Decker 1997). Our new AHe data with the majority of ages ranging from 11 to 6 Ma clearly corroborate that not enough tectonic and/or erosional exhumation has occurred since then to be recorded by low-temperature thermochronology. Thus, our findings do not support an orogen-wide drastic increase in denudation during Pliocene and Pleistocene times.

Conclusions

- AHe data from the eastern Periadriatic fault reveal a Late Miocene phase of activity and exhumation leading to the formation of the Karawanken flower structure and the infill of the Klagenfurt basin.
- New thermochronological data from the central-eastern Southern Alps constrain a coeval phase of uplift and erosion during the latest Mid- to Late Miocene.
- Mid- to Late Miocene AHe cooling ages from the Valsugana thrust, the Val Trompia thrust, the Tonale fault and the Giudicarie belt in the Southern Alps indicate at least 2 km of exhumation since then. Along thrust systems (i.e., Valsugana and Val Trompia thrusts) uplift and erosion were larger as demonstrated by Miocene AFT ages.
- However, even along the thrusts exhumation can be highly differential, as shown for the western sector of the Valsugana thrust.
- Exhumation and deformation related to Adria indentation was initially confined within the orogenic core of the Eastern Alps, the Tauern Window, but became more widespread during Mid- to Late Miocene times.

- This shift from focused exhumation outside the indenter to exhumation within, and deformation of the indenter, is ascribed to a major shift in the coupling state, from a decoupled to a coupled system.

References

Ault AK, Flowers RM (2012) Is apatite U–Th zonation information necessary for accurate interpretation of apatite (U–Th)/He thermochronometry data? Geochim Cosmochim Acta 79:60–78. doi:10.1016/j.gca.2011.11.037

Bada G, Horvath F, Cloetingh S, Coblentz DD, Toth T (2001) Role of topography-induced gravitational stresses in basin inversion: the case study of the Pannonian basin. Tectonics 20:343–363. doi:10.1029/2001tc900001

Baran R, Friedrich AM, Schlunegger F (2014) The late Miocene to Holocene erosion pattern of the Alpine foreland basin reflects Eurasian slab unloading beneath the western Alps rather than global climate change. Lithosphere 6:124–131. doi:10.1130/L307.1

Barbieri G, Grandesso P (2007) Note illustrative della Carta Geologica d'Italia alla scale 1:50.000. Foglio 082 Asiago. APAT., S.EL.CA. s.r.l., Firenze, 135 pp

Bartel EM, Neubauer F, Genser J, Heberer B (2014a) States of paleostress north and south of the Periadriatic fault: comparison of the Drau Range and the Friuli Southalpine wedge. Tectonophysics 637:305–327. doi:10.1016/j.tecto.2014.10.019

Bartel EM, Neubauer F, Heberer B, Genser J (2014b) A low-temperature ductile shear zone: the gypsum-dominated western extension of the brittle Fella-Sava Fault, Southern Alps. J Struct Geol 69:18–31. doi:10.1016/j.jsg.2014.09.016

Battaglia M, Murray MH, Serpelloni E, Burgmann R (2004) The Adriatic region: an independent microplate within the Africa–Eurasia collision zone. Geophys Res Lett. doi:10.1029/2004gl019723

Behrmann JH (1988) Crustal-scale extension in a convergent orogen—the Sterzing–Steinach Mylonite Zone in the Eastern Alps. Geodin Acta 2:63–73. doi:10.1080/09853111.1988.11105157

Bernet M, Brandon M, Garver J, Balestieri ML, Ventura B, Zattin M (2009) Exhuming the Alps through time: clues from detrital zircon fission-track thermochronology. Basin Res 21:781–798. doi:10.1111/j.1365-2117.2009.00400.x

Bertotti G, Seward D, Wijbrans J, ter Voorde M, Hurford AJ (1999) Crustal thermal regime prior to, during, and after rifting: a geochronological and modeling study of the Mesozoic South Alpine rifted margin. Tectonics 18:185–200. doi:10.1029/1998TC900028

Bertrand A (2013) Exhuming the core of collisional orogens, the Tauern Window (Eastern-Alps). Dissertation, FU Berlin

Bertrand A, Rosenberg C, Garcia S (2015) Fault slip analysis and late exhumation of the Tauern Window, Eastern Alps. Tectonophysics 649:1–17. doi:10.1016/j.tecto.2015.01.002

Bigi G, Cosentino D, Parotto M, Sartori R, Scandone P (1990) Structural model of Italy and gravity map (1:500 000). Quad. Ric. Sci. SELCA, Firenze

Bosellini A, Doglioni C (1986) Inherited Structures in the Hangingwall of the Valsugana Overthrust (Southern Alps, Northern Italy). J Struct Geol 8:581–583. doi:10.1016/0191-8141(86)90007-6

Brack P (1981) Structures in the northwestern border of the Adamello intrusion (Alpi Bresciane, Italy). Schweiz Mineral Petrogr Mitt 61:37–50

Bressan G, Snidarcig A, Venturini C (1998) Present state of tectonic stress of the Friuli area (eastern Southern Alps). Tectonophysics 292:211–227. doi:10.1016/S0040-1951(98)00065-1

Brügel A, Dunkl I, Frisch W, Kuhlemann J, Balogh K (2003) Geochemistry and geochronology of gneiss pebbles from foreland Molasse conglomerates: geodynamic and paleogeographic implications for the Oligo-Miocene evolution of the Eastern Alps. J Geol 111:543–563. doi:10.1086/376765

Campani M, Mancktelow N, Seward D, Rolland Y, Muller W, Guerra I (2010) Geochronological evidence for continuous exhumation through the ductile-brittle transition along a crustal-scale low-angle normal fault: simplon Fault Zone, central Alps. Tectonics. doi:10.1029/2009tc002582

Caporali A, Neubauer F, Ostini L, Stangl G, Zuliani D (2013) Modeling surface GPS velocities in the Southern and Eastern Alps by finite dislocations at crustal depths. Tectonophysics 590:136–150. doi:10.1016/j.tecto.2013.01.016

Caputo R, Bosellini A (1994) La flessura pedemontana del Veneto centrale: anticlinale da rampa a sviluppo bloccato. Atti Tic Sc Terra Ser Spec 1:255–268

Caputo R, Poli ME, Zanferrari A (2010) Neogene-Quaternary tectonic stratigraphy of the eastern Southern Alps, NE Italy. J Struct Geol 32:1009–1027. doi:10.1016/J.Jsg.2010.06.004

Carlson WD, Donelick RA, Ketcham RA (1999) Variability of apatite fission-track annealing kinetics; I, experimental results. Am Mineral 84:1213–1223

Castellarin A, Cantelli L (2000) Neo-Alpine evolution of the Southern Eastern Alps. J Geodyn 30:251–274. doi:10.1016/S0264-3707(99)00036-8

Castellarin A, Fesce AM, Picotti V, Pini GA, Prosser G, Sartori R, Selli L, Cantelli L, Ricci R (1988) Stuctural and kinematic analysis of the Giudicarie deformation belt. Implications for compressional tectonics of the Southern Alps. Min Pet Acta 30:287–310

Castellarin A, Cantelli L, Fesce AM, Mercier JL, Picotti V, Pini GA, Prosser G, Selli L (1992) Alpine compressional tectonics in the Southern Alps. Relationships with the N-Apennines. Ann Tecton VI:62–94

Castellarin A, Piccioni S, Prosser G, Sanguinetti E, Sartori R, Selli L (1993) Mesozoic continental rifting and Neogene inversion along the South Giudicarie Line (Northwestern Brenta Dolomites). Mem Soc Geol It 49:125–144

Castellarin A, Vai GB, Cantelli L (2006) The alpine evolution of the Southern Alps around the Giudicarie faults: a Late Cretaceous to Early Eocene transfer zone. Tectonophysics 414:203–223. doi:10.1016/J.Tecto.2005.10.019

Cederbom CE, Sinclair HD, Schlunegger F, Rahn MK (2004) Climate-induced rebound and exhumation of the European Alps. Geology 32:709–712. doi:10.1130/G20491.1

Cliff R, Holzer HF, Rex DC (1974) The age of Eisenkappel granite and the history of the Periadriatic Lineament. Verh Geol Bundesanstalt 2(3):347–350

D'Adda P, Zanchi A, Bergomi M, Berra F, Malusa MG, Tunesi A, Zanchetta S (2011) Polyphase thrusting and dyke emplacement in the central Southern Alps (Northern Italy). Int J Earth Sci 100:1095–1113. doi:10.1007/s00531-010-0586-2

Dal Piaz GV, Castellarin A, Martin S, Selli L, Carton A, Pellegrini GB, Casolari E, Daminato F, Montresor L, Picotti V (2007) Note Illustrative della Carta Geologica d'Italia alla scala 1:50.000, Foglio 042 Malé. Provincia Autonoma di Trento, Servizio Geologico. APAT, Servizio Geologico d'Italia, Roma

Doglioni C, Bosellini A (1987) Eoalpine and mesoalpine tectonics in the Southern Alps. Geol Rundschau 76:735–754

Dunkl I, Frisch W, Grundmann G (2003) Zircon fission track thermochronology of the southeastern part of the Tauern Window and the adjacent Austroalpine margin. Eclogae Geol Helvetiae 96:209–217

Emmerich A, Glasmacher UA, Bauer F, Bechstadt T, Zuhlke R (2005) Meso-/Cenozoic basin and carbonate platform development in the SW-Dolomites unraveled by basin modelling and apatite FT analysis: rosengarten and Latemar (Northern Italy). Sediment Geol 175:415–438. doi:10.1016/j.sedgeo.2004.12.022

Exner C (1976) Die geologische Position der Magmatite des periadriatischen Lineamentes. Verh Geol Bundesanstalt H. 2:3–64

Farley KA (2002) (U–Th)/He dating: techniques, calibrations, and applications. Mineral Soc Am Rev Mineral Geochem 47:819–844. doi:10.2138/rmg.2002.47.18

Favaro S, Schuster R, Handy MR, Scharf A, Pestal G (2015) Transition from orogen-perpendicular to orogen-parallel exhumation and cooling during crustal indentation—key constraints from 147Sm/144Nd and 87Rb/87Sr geochronology (Tauern Window, Alps). Tectonophysics 665:1–16. doi:10.1016/j.tecto.2015.08.037

Fitzgerald PG, Baldwin SL, Webb LE, O'Sullivan PB (2006) Interpretation of (U–Th)/He single grain ages from slowly cooled crustal terranes: a case study from the Transantarctic Mountains of southern Victoria Land. Chem Geol 225:91–120. doi:10.1016/j.chemgeo.2005.09.001

Flowers RM, Ketcham RA, Shuster DL, Farley KA (2009) Apatite (U–Th)/He thermochronometry using a radiation damage accumulation and annealing model. Geochim Cosmochim Acta 73:2347–2365. doi:10.1016/j.gca.2009.01.015

Fodor L, Jelen B, Márton E, Skaberne D, Car J, Vrabec M (1998) Miocene–Pliocene tectonic evolution of the Slovenian Periadriatic fault: implications for Alpine–Carpathian extrusion models. Tectonics 17:690–709. doi:10.1029/98tc01605

Fodor L, Gerdes A, Dunkl I, Koroknai B, Pécskay Z, Trajanova M, Horváth P, Vrabec M, Jelen B, Balogh K, Frisch W (2008) Miocene emplacement and rapid cooling of the Pohorje pluton at the Alpine–Pannonian–Dinaridic junction, Slovenia. Swiss J Geosci 101:S255–S271. doi:10.1007/S00015-008-1286-9

Foeken JPT, Persano C, Stuart FM, ter Voorde M (2007) Role of topography in isotherm perturbation: apatite (U–Th)/He and fission track results from the Malta tunnel, Tauern Window, Austria. Tectonics. doi:10.1029/2006tc002049

Fox M, Herman F, Kissling E, Willett SD (2015) Rapid exhumation in the Western Alps driven by slab detachment and glacial erosion. Geology 43:379–382. doi:10.1130/G36411.1

Frisch W, Kuhlemann J, Dunkl I, Brugel A (1998) Palinspastic reconstruction and topographic evolution of the eastern Alps during late Tertiary tectonic extrusion. Tectonophysics 297:1–15. doi:10.1016/S0040-1951(98)00160-7

Frisch W, Dunkl I, Kuhlemann J (2000) Post-collisional orogen-parallel large-scale extension in the Eastern Alps. Tectonophysics 327:239–265. doi:10.1016/S0040-1951(00)00204-3

Fügenschuh B, Seward D, Mancktelow N (1997) Exhumation in a convergent orogen: the western Tauern window. Terra Nova 9:213–217. doi:10.1111/j.1365-3121.1997.tb00015.x

Gebrande H, Lüschen E, Bopp M, Bleibinhaus F, Lammerer B, Oncken O, Stiller M, Kummerow J, Kind R, Millahn K, Grassl H, Neubauer F, Bertelli L, Borrini D, Fantoni R, Pessina C, Sella M, Castellarin A, Nicolich R, Mazzotti A, Bernabini M, Grp TW (2002) First deep seismic reflection images of the Eastern Alps reveal giant crustal wedges and transcrustal ramps. Geophys Res Lett. doi:10.1029/2002gl014911

Genser J, Cloetingh SAPL, Neubauer F (2007) Late orogenic rebound and oblique Alpine convergence: new constraints from subsidence analysis of the Austrian Molasse basin. Global Planet Change 58:214–223. doi:10.1016/J.Gloplacha.2007.03.010

Glotzbach C, van der Beek PA, Spiegel C (2011) Episodic exhumation and relief growth in the Mont Blanc massif, Western Alps from numerical modelling of thermochronology data. Earth Planet Sci Lett 304:417–430. doi:10.1016/J.Epsl.2011.02.020

Green PF, Duddy IR (2006) Interpretation of apatite (U–Th)/He ages and fission track ages from cratons. Earth Planet Sci Lett 244:541–547. doi:10.1016/j.epsl.2006.02.024

Grenerczy G, Sella G, Stein S, Kenyeres A (2005) Tectonic implications of the GPS velocity field in the northern Adriatic region. Geophys Res Lett. doi:10.1029/2005gl022947

Grobe A, Littke R, Sachse V, Leythaeuser D (2015) Burial history and thermal maturity of Mesozoic rocks of the Dolomites, Northern Italy. Swiss J Geosci 108:253–271. doi:10.1007/s00015-015-0191-2

Gusterhuber J, Dunkl I, Hinsch R, Linzer HG, Sachsenhofer RF (2012) Neogene uplift and erosion in the Alpine Foreland Basin (Upper Austria and Salzburg). Geol Carpath 63:295–305. doi:10.2478/V10096-012-0023-5

Handy MR, Schmid SM, Bousquet R, Kissling E, Bernoulli D (2010) Reconciling plate-tectonic reconstructions of Alpine Tethys with the geological–geophysical record of spreading and subduction in the Alps. Earth Sci Rev 102:121–158. doi:10.1016/j.earscirev.2010.06.002

Handy MR, Ustaszewski K, Kissling E (2014) Reconstructing the Alps–Carpathians–Dinarides as a key to understanding switches in subduction polarity, slab gaps and surface motion. Int J Earth Sci 104:1–26. doi:10.1007/s00531-014-1060-3

Häuselmann P, Mihevc A, Pruner P, Horacek I, Cermak S, Hercman H, Sahy D, Fiebig M, Hajna NZ, Bosak P (2015) Snezna jama (Slovenia): interdisciplinary dating of cave sediments and implication for landscape evolution. Geomorphology 247:10–24. doi:10.1016/j.geomorph.2014.12.034

Hejl E (1997) 'Cold spots' during the Cenozoic evolution of the Eastern Alps: thermochronological interpretation of apatite fission-track data. Tectonophysics 272:159–173. doi:10.1016/S0040-1951(96)00256-9

Hergarten S, Wagner T, Stuwe K (2010) Age and prematurity of the Alps derived from topography. Earth Planet Sci Lett 297:453–460. doi:10.1016/J.Epsl.2010.06.048

Herman F, Seward D, Valla PG, Carter A, Kohn B, Willett SD, Ehlers T (2013) Worldwide acceleration of mountain erosion under a cooling climate. Nature 504:423–426. doi:10.1038/nature12877

Horváth F, Cloetingh S (1996) Stress-induced late-stage subsidence anomalies in the Pannonian basin. Tectonophysics 266:287–300. doi:10.1016/S0040-1951(96)00194-1

House MA, Kohn BP, Farley KA, Raza A (2002) Evaluating thermal history models for the Otway Basin, southeastern Australia, using (U–Th)/He and fission-track data from borehole apatites. Tectonophysics 349:277–295. doi:10.1016/S0040-1951(02)00057-4

Hurford AJ, Green PF (1983) The zeta age calibration of fission-track dating. Chem Geol 41:285–317. doi:10.1016/S0009-2541(83)80026-6

Keim L, Stingl V (2000) Lithostratigraphy and facies architecture of the Oligocene conglomerates at Monte Parei (Fanes, Dolomites, Italy). Riv Ital Paleontol S 106:123–131

Klaus W (1956) Mikrosporenhorizonte in Süd- und Ostkärnten. Verh Geol Bundesanstalt 1956:250–255

Kuhlemann J, Frisch W, Szekely B, Dunkl I, Kazmer M (2002) Post-collisional sediment budget history of the Alps: tectonic versus climatic control. Int J Earth Sci 91:818–837. doi:10.1007/S00531-002-0266-Y

Kurz W, Neubauer F (1996) Deformation partitioning during updoming of the Sonnblick area in the Tauern Window (Eastern Alps, Austria). J Struct Geol 18:1327–1343. doi:10.1016/S0191-8141(96)00057-0

Lammerer B, Gebrande H, Lüschen E, Vesela P (2008) A crustal-scale cross section through the Tauern Window (eastern Alps) from geophysical and geological data. In: Siegesmund S et al (eds) Tectonic aspects of the Alpine–Dinaride–Carpathian system, vol 298. Geological Society, Special Publications, London, pp 219–229. doi:10.1144/SP298.11

Laubscher H (1983) The late Alpine (Periadriatic) intrusions and the Insubric Line. Mem Soc Geol It 26:21–30

Läufer AL, Frisch W, Steinitz G, Loeschke J (1997) Exhumed fault-bounded Alpine blocks along the Periadriatic lineament: the Eder unit (Carnic Alps, Austria). Geol Rundsch 86:612–626. doi:10.1007/s005310050167

Legrain N, Stüwe K, Wolfler A (2014) Incised relict landscapes in the eastern Alps. Geomorphology 221:124–138. doi:10.1016/J.Geomorph.2014.06.010

Legrain N, Dixon J, Stuwe K, von Blanckenburg F, Kubik P (2015) Post-Miocene landscape rejuvenation at the eastern end of the Alps. Lithosphere 7:3–13. doi:10.1130/L391.1

Lippitsch R, Kissling E, Ansorge J (2003) Upper mantle structure beneath the Alpine orogen from high-resolution teleseismic tomography. J Geophys Res Sol Earth. doi:10.1029/2002JB002016

Luth SW, Willingshofer E (2008) Mapping of the post-collisional cooling history of the Eastern Alps. Swiss J Geosci 101:207–223. doi:10.1007/S00015-008-1294-9

Mahéo G, Gautheron C, Leloup PH, Fox M, Tassant-Got L, Douville E (2013) Neogene exhumation history of the Bergell massif (southeast Central Alps). Terra Nova 25:110–118. doi:10.1111/ter.12013

Mancktelow NS (1992) Neogene lateral extension during convergence in the Central Alps—evidence from interrelated faulting and backfolding around the Simplon pass (Switzerland). Tectonophysics 215:295–317. doi:10.1016/0040-1951(92)90358-D

Martin S, Bigazzi G, Zattin M, Viola G, Balestrieri ML (1998) Neogene kinematics of the Giudicarie fault (Central-Eastern Alps, Italy): new apatite fission-track data. Terra Nova 10:217–221. doi:10.1046/j.1365-3121.1998.00119.x

Massari F, Grandesso P, Stefani C, Zanferrari A (1986) The Oligo-Miocene Molasse of the Veneto-Friuli region, Southern Alps. Giorn Geol 48:235–255

Massironi M, Zampieri D, Caporali A (2006) Miocene to present major fault linkages through the Adriatic indenter and the Austroalpine–Penninic collisional wedge (Alps of NE Italy). Geolo Soc Lond Spec Publ 262:245–258. doi:10.1144/GSL.SP.2006.262.01.15

Mellere D, Stefani C, Angevine C (2000) Polyphase tectonics through subsidence analysis: the Oligo-miocene Venetian and Friuli Basin, north-east Italy. Basin Res 12:159–182. doi:10.1046/j.1365-2117.2000.00120.x

Miller C, Thoni M, Goessler W, Tessadri R (2011) Origin and age of the Eisenkappel gabbro to granite suite (Carinthia, SE Austrian Alps). Lithos 125:434–448. doi:10.1016/j.lithos.2011.03.003

Monegato G, Stefani C (2010) Stratigraphy and evolution of a long-lived fluvial system in the Southeastern Alps (NE Italy): the Tagliamento Conglomerate. Austrian J Earth Sci 103:33–49

Naeser CW (1979) Fission-track dating and geologic annealing of fission tracks. In: Jäger E, Hunziker J (eds) Lectures in isotope geology. Springer, Berlin, pp 154–169

Nemes F (1996) Kinematics of the Periadriatic fault in the Eastern Alps—evidence from structural analysis, fission track dating and basin modelling. Dissertation, University of Salzburg pp

Nemes F, Neubauer F, Cloetingh S, Genser J (1997) The Klagenfurt Basin in the Eastern Alps: an intra-orogenic decoupled flexural basin? Tectonophysics 282:189–203. doi:10.1016/S0040-1951(97)00219-9

Peresson H, Decker K (1997) Far-field effect of Late Miocene subduction in the eastern Carpathians: E–W compression and inversion of structures in the Alpine–Carpathian–Pannonian region. Tectonics 16:38–56. doi:10.1029/96tc02730

Picotti V, Prosser G, Castellarin A (1995) Structure and kinematics of the Giudicarie–Val Trompia Fold and Thrust Belt (Central Southern Alps, Northern Italy). Mem Soc Geol It 47:45–109

Pieri M, Groppi G (1981) Subsurface geological structure of the Po Plain, Publication 414 del Progetto Finalizzato Geodinamica. CNR. Internal report

Piller WE, Harzhauser M, Mandic O (2007) Miocene Central Paratethys stratigraphy—current status and future directions. Stratigraphy 4:151–168

Polinski RK, Eisbacher GH (1992) Deformation partitioning during polyphase oblique convergence in the Karawanken Mountains, Southeastern Alps. J Struct Geol 14:1203–1213. doi:10.1016/0191-8141(92)90070-D

Pomella H, Klötzli U, Scholger R, Stipp M, Fügenschuh B (2011) The Northern Giudicarie and the Meran-Mauls fault (Alps, Northern Italy) in the light of new paleomagnetic and geochronological data from boudinaged Eo-/Oligocene tonalites. Int J Earth Sci 100:1827–1850. doi:10.1007/S00531-010-0612-4

Pomella H, Stipp M, Fügenschuh B (2012) Thermochronological record of thrusting and strike-slip faulting along the Giudicarie fault system (Alps, Northern Italy). Tectonophysics 579:118–130. doi:10.1016/J.Tecto.2012.04.015

Prosser G (1998) Strike-slip movements and thrusting along a transpressive fault zone: the North Giudicarie line (Insubric line, northern Italy). Tectonics 17:921–937. doi:10.1029/1998TC900010

Ratschbacher L, Frisch W, Linzer HG, Merle O (1991) Lateral extrusion in the Eastern Alps, 2. Structural-analysis. Tectonics 10:257–271. doi:10.1029/90TC02622

Reiners PW, Farley KA (2001) Influence of crystal size on apatite (U–Th)/He thermochronology: an example from the Bighorn Mountains, Wyoming. Earth Planet Sci Lett 188:413–420. doi:10.1016/S0012-821X(01)00341-7

Reverman RL, Fellin MG, Herman F, Willett SD, Fitoussi C (2012) Climatically versus tectonically forced erosion in the Alps: thermochronometric constraints from the Adamello Complex, Southern Alps, Italy. Earth Planet Sci Lett 339:127–138. doi:10.1016/j.epsl.2012.04.051

Robl J, Stüwe K (2005) Continental collision with finite indenter strength: 2. European Eastern Alps. Tectonics. doi:10.1029/2004tc001741

Robl J, Hergarten S, Stüwe K (2008) Morphological analysis of the drainage system in the Eastern Alps. Tectonophysics 460:263–277. doi:10.1016/j.tecto.2008.08.024

Robl J, Prasicek G, Hergarten S, Stüwe K (2015) Alpine topography in the light of tectonic uplift and glaciation. Glob Planet Change 127:34–49. doi:10.1016/j.gloplacha.2015.01.008

Rosenberg CL, Berger A (2009) On the causes and modes of exhumation and lateral growth of the Alps. Tectonics. doi:10.1029/2008tc002442

Rosenberg CL, Berger A, Bellahsen N, Bousquet R (2015) Relating orogen width to shortening, erosion, and exhumation during Alpine collision. Tectonics 34:1306–1328. doi:10.1002/2014TC003736

Sachsenhofer RF, Lankreijer A, Cloetingh S, Ebner F (1997) Subsidence analysis and quantitative basin modelling in the Styrian basin (Pannonian basin system, Austria). Tectonophysics 272:175–196. doi:10.1016/S0040-1951(96)00257-0

Sachsenhofer RF, Jelen B, Hasenhuttl C, Dunkl I, Rainer T (2001) Thermal history of tertiary basins in Slovenia (Alpine–Dinaride–Pannonian junction). Tectonophysics 334:77–99. doi:10.1016/S0040-1951(01)00057-9

Scharbert S (1975) Radiometrische Altersbestimmungen von Intrusivgesteinen im Raum Eisenkappel (Karanwanken, Kärnten). Verh Geol Bundesanstalt 4:301–304

Scharf A, Handy MR, Favaro S, Schmid SM, Bertrand A (2013) Modes of orogen-parallel stretching and extensional exhumation in response to microplate indentation and roll-back subduction (Tauern Window, Eastern Alps). Int J Earth Sci 102:1627–1654. doi:10.1007/S00531-013-0894-4

Schmid S, Aebli HR, Heller F, Zingg A (1987) The role of the Periadriatic Line in the tectonic evolution of the Alps. In: Coward MP, Dietrich D (eds) Alpine tectonics, vol 45. Geological Society London Special Publication, London, pp 153–171

Schmid SM, Pfiffner OA, Froitzheim N, Schonborn G, Kissling E (1996) Geophysical–geological transect and tectonic evolution of the Swiss-Italian Alps. Tectonics 15:1036–1064. doi:10.1029/96tc00433

Schmid SM, Scharf A, Handy MR, Rosenberg CL (2013) The Tauern Window (Eastern Alps, Austria): a new tectonic map, with cross-sections and a tectonometamorphic synthesis. Swiss J Geosci 106:1–32. doi:10.1007/S00015-013-0123-Y

Schneider S, Hammerschmidt K, Rosenberg CL, Gerdes A, Frei D, Bertrand A (2015) U–Pb ages of apatite in the western Tauern Window (Eastern Alps): tracing the onset of collision-related exhumation in the European plate. Earth Planet Sci Lett 418:53–65. doi:10.1016/j.epsl.2015.02.020

Schoenborn G (1992) Alpine tectonics and kinematic models of the central Southern Alps. Mem Soc Geol It 44:229–393

Sciunnach DAB (1994) Plagioclase-arenites in the Molveno Lake area (Trento): record of an Eocene volcanic arc. Studi Trentini Sci Nat Acta Geol 69:81–92

Selli L (1998) Il llineamento della Valsugana fra Trento e Cima d'Asta: cinematica neogenica ed eredita' strutturali permo-mesozoiche nel quadro evolutivo del Sudalpino orientale (NE-Italia). Mem Soc Geol lt 53:503–541

Shuster DL, Farley KA (2009) The influence of artificial radiation damage and thermal annealing on helium diffusion kinetics in apatite. Geochim Cosmochim Acta 73:183–196. doi:10.1016/j.gca.2008.10.013

Shuster DL, Flowers RM, Farley KA (2006) The influence of natural radiation damage on helium diffusion kinetics in apatite. Earth Planet Sci Lett 249:148–161. doi:10.1016/j.gca.2008.10.013

Spada M, Bianchi I, Kissling E, Agostinetti NP, Wiemer S (2013) Combining controlled-source seismology and receiver function information to derive 3-D Moho topography for Italy. Geophys J Int 194:1050–1068. doi:10.1093/gji/ggt148

Spalla MI, Gosso G (1999) Pre-Alpine tectonometamorphic units in the central southern Alps; structural and metamorphic memory. Mem Sci Geol 51:221–229

Spiegel C, Kohn B, Belton D, Berner Z, Gleadow A (2009) Apatite (U–Th–Sm)/He thermochronology of rapidly cooled samples: the effect of He implantation. Earth Planet Sci Lett 285:105–114. doi:10.1016/j.epsl.2009.05.045

Staufenberg H (1987) Apatite fission-track evidence for postmetamorphic uplift and cooling history of the eastern Tauern Window and the surrounding Austroalpine (Central Eastern Alps, Austria). Jb Geol Bundesanstalt 13:571–586

Stipp M, Stünitz H, Heilbronner R, Schmid SM (2002) The eastern Tonale fault zone: a 'natural laboratory' for crystal plastic deformation of quartz over a temperature range from 250 to 700 °C. J Struct Geol 24:1861–1884. doi:10.1016/S0191-8141(02)00035-4

Stipp M, Fügenschuh B, Gromet LP, Stünitz H, Schmid SM (2004) Contemporaneous plutonism and strike-slip faulting: a case study from the Tonale fault zone north of the Adamello pluton (Italian Alps). Tectonics. doi:10.1029/2003TC001515

Tapponnier M, Peltzer G, Armijo R (1986) On the mechanics of the collision between India and Asia. Geol Soc London Spec Publ 19:113–157. doi:10.1144/GSL.SP.1986.019.01.07

Tollmann A (1985) Geologie von Österreich, Bd.II: Außerzentralalpiner Teil. Deuticke, Wien, 710 p

Tomljenovic B, Csontos L (2001) Neogene-quaternary structures in the border zone between Alps, Dinarides and Pannonian Basin (Hrvatsko zagorje and Karlovac Basins, Croatia). Int J Earth Sci 90:560–578. doi:10.1007/S005310000176

van Gelder IE, Matenco L, Willingshofer E, Tomljenovic B, Andriessen PAM, Ducea MN, Beniest A, Gruić A (2015) The tectonic evolution of a critical segment of the Dinarides–Alps connection : kinematic and geochronological inferences from the Medvednica Mountains, NE Croatia. Tectonics 34:1952–1978. doi:10.1002/2015TC003937

Venzo S (1977) I depositi quaternari e del Neogene superiore nella bassa Valle del Piave da Quero al Montello e del Paleo-Piave nella valle del Soligo. Mem Ist Geol Mineral Univ Padova 30:64

Vigano A, Bressan G, Ranalli G, Martin S (2008) Focal mechanism inversion in the Giudicarie–Lessini seismotectonic region (Southern Alps, Italy): insights on tectonic stress and strain. Tectonophysics 460:106–115. doi:10.1016/j.tecto.2008.07.008

Viola G (2000) Kinematics and timing of the Periadriatic fault system in the Giudicarie region (central-eastern Alps). Dissertation, ETH Zürich

Viola G, Mancktelow NS, Seward D (2001) Late Oligocene–Neogene evolution of Europe-Adria collision: new structural and geochronological evidence from the Giudicarie fault system (Italian Eastern Alps). Tectonics 20:999–1020. doi:10.1029/2001TC900021

Viola G, Mancktelow NS, Seward D, Meier A, Martin S (2003) The Pejo fault system: an example of multiple tectonic activity in the Italian Eastern Alps. Geol Soc Am Bull 115:515–532. doi:10.1130/0016-7606(2003)115<0515:TPFSAE>2.0.CO;2

von Blanckenburg F, Davies JH (1995) Slab breakoff—a model for syncollisional magmatism and tectonics in the Alps. Tectonics 14:120–131. doi:10.1029/94tc02051

von Gosen W (1989) Fabric developments and the evolution of the Periadriatic Lineament in southeast Austria. Geol Mag 126:55–71. doi:10.1017/S0016756800006142

Wagner T, Fabel D, Fiebig M, Hauselmann P, Sahy D, Xu S (2010) Stuwe K (2010) Young uplift in the non-glaciated parts of the Eastern Alps. Earth Planet Sci Lett 295:159–169. doi:10.1016/J.Epsl.2010.03.034

Willett SD, Schlunegger F, Picotti V (2006) Messinian climate change and erosional destruction of the central European Alps. Geology 34:613–616. doi:10.1130/G22280.1

Willingshofer E, Cloetingh S (2003) Present-day lithospheric strength of the Eastern Alps and its relationship to neotectonics. Tectonics. doi:10.1029/2002TC001463

Willingshofer E, Sokoutis D (2009) Decoupling along plate boundaries: key variable controlling the mode of deformation and the

geometry of collisional mountain belts. Geology 37:39–42. doi:10.1130/G25321A.1

Wolf RA, Farley KA, Silver LT (1996) Helium diffusion and low-temperature thermochronometry of apatite. Geochim Cosmochim Ac 60:4231–4240. doi:10.1016/S0016-7037(96)00192-5

Wolff R, Dunkl I, Kiesselbach G, Wemmer K, Siegesmund S (2012) Thermochronological constraints on the multiphase exhumation history of the Ivrea–Verbano Zone of the Southern Alps. Tectonophysics 579:104–117. doi:10.1016/j.tecto.2012.03.019

Wölfler A, Dekant C, Danisik M, Kurz W, Dunkl I, Putis M, Frisch W (2008) Late stage differential exhumation of crustal blocks in the central Eastern Alps: evidence from fission track and (U–Th)/He thermochronology. Terra Nova 20:378–384. doi:10.1111/J.1365-3121.2008.00831.X

Wölfler A, Kurz W, Danisik M, Rabitsch R (2010) Dating of fault zone activity by apatite fission track and apatite (U–Th)/He thermochronometry: a case study from the Lavanttal fault system (Eastern Alps). Terra Nova 22:274–282. doi:10.1111/J.1365-3121.2010.00943.X

Wölfler A, Kurz W, Fritz H, Stüwe K (2011) Lateral extrusion in the Eastern Alps revisited: refining the model by thermochronological, sedimentary, and seismic data. Tectonics. doi:10.1029/2010TC002782

Wölfler A, Stüwe K, Danisik M, Evans NJ (2012) Low temperature thermochronology in the Eastern Alps: implications for structural and topographic evolution. Tectonophysics 541:1–18. doi:10.1016/J.Tecto.2012.03.016

Zampieri D, Massironi M (2007) Evolution of a poly-deformed relay zone between fault segments in the eastern Southern Alps, Italy. In: Cunningham WD, Mann P (eds) Tectonics of strike-slip restraining and releasing bends, vol 290. Geological Society Special Publications, London, pp 351–366. doi:10.1144/SP290.13

Zanchetta S, D'Adda P, Zanchi A, Barberini V, Villa IM (2011) Cretaceous–Eocene compression in the central Southern Alps (N Italy) inferred from Ar-40/Ar-39 dating of pseudotachylytes along regional thrust faults. J Geodyn 51:245–263. doi:10.1016/j.jog.2010.09.004

Zanchetta S, Malusa MG, Zanchi A (2015) Precollisional development and Cenozoic evolution of the Southalpine retrobelt (European Alps). Lithosphere Us 7:662–681. doi:10.1130/L466.1

Zattin M, Stefani C, Martin S (2003) Detrital fission-track analysis and sedimentary petrofacies as keys of Alpine exhumation; the example of the Venetian foreland (European Southern Alps, Italy). J Sediment Res 73:1051–1061. doi:10.1306/051403731051

Zattin M, Cuman A, Fantoni R, Martin S, Scotti P, Stefani C (2006) From Middle Jurassic heating to Neogene cooling: the thermochronological evolution of the southern Alps. Tectonophysics 414:191–202. doi:10.1016/J.Tecto.2005.10.020